HHS Public Access

Author manuscript

Nature. Author manuscript; available in PMC 2021 August 25.

Published in final edited form as:

Nature. 2021 March ; 591(7848): 99–104. doi:10.1038/s41586-020-03169-5.

Structural and developmental principles of neuropil assembly in *C. elegans*

Mark W. Moyle[1], **Kristopher M. Barnes**[2], **Manik Kuchroo**[3], **Alex Gonopolskiy**[3], **Leighton H. Duncan**[1], **Titas Sengupta**[1], **Lin Shao**[1], **Min Guo**[4], **Anthony Santella**[2], **Ryan Christensen**[4], **Abhishek Kumar**[5], **Yicong Wu**[4], **Kevin R. Moon**[6], **Guy Wolf**[7], **Smita Krishnaswamy**[3,*], **Zhirong Bao**[2,*], **Hari Shroff**[4,8,*], **William A. Mohler**[9,*], **Daniel A. Colón-Ramos**[1,8,10,*,^]

[1]Department of Neuroscience and Department of Cell Biology, Yale University School of Medicine, New Haven, CT 06536, USA.

[2]Developmental Biology Program, Sloan Kettering Institute, New York, NY 10065, USA.

[3]Department of Genetics, Yale University School of Medicine, New Haven, CT 06520, USA.

[4]Laboratory of High Resolution Optical Imaging, National Institute of Biomedical Imaging and Bioengineering, National Institutes of Health, Bethesda, MD 20892, USA.

[5]Marine Biological Laboratory, Woods Hole, MA 02543, USA.

[6]Department of Mathematics and Statistics, Utah State University, Logan, UT 84322, USA.

[7]Department of Mathematics and Statistics, Université de Montréal, Montréal, Quebec H3T 1J4, Canada.

[8]MBL Fellows, Marine Biological Laboratory, Woods Hole, MA 02543, USA

[9]Department of Genetics and Genome Sciences and Center for Cell Analysis and Modeling, University of Connecticut Health Center, Farmington, CT 06030, USA.

[10]Instituto de Neurobiología, Recinto de Ciencias Médicas, Universidad de Puerto Rico, San Juan 00901, Puerto Rico.

^Correspondence and request for materials should be addressed to D.A.C.R. Daniel A. Colón-Ramos, Ph.D., Department of Neuroscience, Department of Cell Biology, Yale University School of Medicine, 333 Cedar Street, SHM B 163D, New Haven, CT 06510, daniel.colon-ramos@yale.edu.

*These co-senior authors jointly supervised this work

Author Contributions

Designed experiments: M.W.M, K.M.B., M.K., A.G., L.H.D., A.S., K.R.M., G.W., S.K., Z.B., H.S., W.A.M., D.A.C-R. Performed biological experiments: M.W.M, K.M.B., L.H.D. Performed computational experiments: M.W.M, K.M.B., M.K., A.G., A.S., G.W., W.A.M. Generated reagents: M.W.M, L.H.D., T.S. Built instrumentation and analysis software: M.W.M, T.S., L.S., M.G., A.S., A.K., Y.W., W.A.M., Contributed lineaging data and expertise: M.W.M., K.M.B, L.H.D, A.S., R.C., Z.B., W.A.M. Prepared manuscript: M.W.M., W.A.M., D.A.C-R. (with assistance from all authors). Supervised research: S.K., Z.B., H.S., W.A.M., D.A.C-R. Directed research: D.A.C-R.

Competing Financial Interests

The authors declare no competing financial interests.

Code Availability

Electron micrograph segmentation adjacency analysis code is available at https://github.com/cabrittin/volumetric_analysis[18]. Diffusion condensation analysis code is available at https://github.com/agonopol/worm_brain[6]. C-PHATE visualization code is available online at dccphate.wormguides.org/CPHATE_pythonCode.zip.

Supplementary Information is available for this paper.

Abstract

Neuropil is a fundamental form of tissue organization within brains1. In neuropils, densely packed neurons synaptically interconnect into precise circuit architecture[2,3], yet the structural and developmental principles governing this nanoscale precision remain largely unknown[4,5]. Here, we use diffusion condensation, an iterative data coarse-graining algorithm6, to identify nested circuit structures within the *C. elegans* neuropil (called the nerve ring). We show that the nerve ring neuropil is largely organized into four strata composed of related behavioral circuits. The stratified architecture of the neuropil is a geometrical representation of the functional segregation of sensory information and motor outputs, with specific sensory organs and muscle quadrants mapping onto particular neuropil strata. We identify groups of neurons with unique morphologies that integrate information across strata and that create neural structures that cage the strata within the nerve ring. We use high resolution light-sheet microscopy[7,8], coupled with lineage-tracing and cell-tracking algorithms[9,10], to resolve the developmental sequence and reveal principles of cell position, migration and outgrowth that guide stratified neuropil organization. Our results uncover conserved structural design principles underlying nerve ring neuropil architecture and function, and a pioneer-neuron-based, temporal progression of outgrowth that guides the hierarchical development of the layered neuropil. Our findings provide a systematic blueprint for using structural and developmental approaches to understand neuropil organization within brains.

To elucidate structural and developmental principles that govern neuropil assembly, we examined the *C. elegans* nerve ring neuropil, a major site of neuronal integration containing 181 of the 282 somatic neurons in the adult hermaphrodite[3]. The lineage, morphology and synaptic connectivity of all 181 neurons is known[3,11]. Network principles and circuit motifs [12–20] as well as cellular and molecular mechanisms of nerve ring formation[21–24] have been elucidated. Yet, we lack an understanding of the structural design principles that underlie nerve ring neuropil architecture and function, and the developmental sequence that forms this functional structure.

Quantitative analyses of neuropil organization.

To systematically dissect the organization of the nerve ring neuropil, we analyzed previously segmented data[18,19] with over 100,000 instances of neurite-neurite contacts quantified for two published *C. elegans* electron microscopy neuropil datasets[3] (Fig. 1a). We focused on contact profiles instead of synaptic connections to reveal both functional and structural neuropil relationships.

We generated an adjacency matrix by summing all contact surface areas for each possible neuron pair, and applied a novel “Diffusion Condensation” (DC[6]) clustering algorithm to iteratively cluster neurons based on the quantitative similarity of each neuron’s contact profile (Fig. 1a). Unlike other clustering algorithms[25–27], DC condenses data without assuming underlying data structure or forcing a k-way partition. At each iteration DC clusters the data by merging neurons that are within a threshold distance of each other. We then applied C-PHATE, an novel extension of the PHATE[28] visualization method, to generate an interactive 3D visualization of the iterative DC clustering (Fig. 1a,b; Methods). By iteratively condensing datapoints closer to neighbors, DC/C-PHATE outputs dynamically

unveil data relationships at varying scales of granularity, from cell-cell to circuit-circuit interactions.

Quantitative comparisons of DC/C-PHATE outputs revealed similar, but not identical, clustering patterns between a Larva Stage 4 (L4) and an adult hermaphrodite nerve ring reconstructions (Adjusted Rand Index, ARI, of 0.7; Extended Data Fig. 1a,b; Extended Data Fig. 2f,m,n), consistent with previous qualitative descriptions of the stereotyped *C. elegans* nerve ring[3] and recent analyses of neurite adjacency differences[18,19] (Extended Data Fig. 2e). Our quantitative analyses of the DC output differences for the larva and adult EM reconstructions also revealed that differences were underpinned by biologically-relevant changes occurring between these developmental stages (Extended Data Fig. 2a–f,q–s; Supplementary Discussion 3). We also note that comparisons between DC analysis using the contact profiles vs. the synaptic connectome were different and consistent with structural relationships in the nerve ring present in the contact profile dataset, but not represented in the synaptic connectome (Extended Data Fig. 2o–p). Yet, examination of clusters throughout the DC iterations of contact profiles revealed known cell-cell interactions and behavioral circuits (Fig. 1b,c; Extended Data Fig. 3a,b)[13,16,17,29–31]. Together, the contact-based multigranular DC outputs enabled understanding of cell-cell interactions within the context of functional circuits, and functional circuits within the context of higher order neuropil structures.

Modularity scores, a measure of cluster separation[32], were highest in the DC iteration that contained four (L4 dataset) to six (adult dataset) clusters (Fig. 1b; Extended Data Fig. 1a,b; Supplementary Video 1,2; Supplementary Discussion 2). Color-coding the neuron members of the four clusters in the L4 dataset (without unassigned neurons; Methods) within the 3D anatomy of the nerve ring revealed that they correspond to distinct, tightly packed layers of neurons within the greater neuropil. These four layers or strata stack along the anterior-posterior axis of the animal, encircling the pharynx isthmus. We named these S1, S2, S3 and S4 for Stratum 1 etc. (Fig. 1c; Extended Data Fig. 1c–h; Supplementary Video 3). Our findings are consistent with studies that identified an anteroposterior hierarchy of connectivity of the nerve ring[14]. This stratified organization, resolved here at single neurons scale, is reminiscent of laminar organizations in the *Drosophila* nervous system[33], and in the vertebrate retina and cerebral cortex[34,35].

We noted no clear spaces between the laminar boundaries of the individual strata within the tightly bundled neuropil. Yet, we identified additional structural features which indicate that these computationally-identified strata represent biologically-relevant structures. For example, in S1, 32 anterior sensory neurons project axons perpendicular to the neuropil before curling 180° and returning to the anterior limits of the neuropil, where they terminate as synaptic endplates[3,36,37] (Fig. 1d; Extended Data Fig. 4a–d). Remarkably, these neurite loops circumscribed computationally defined boundaries between S2 and S3/S4. The anterior loops encase ~90% of S2, and the posterior loops encase ~84% of S3 and 100% of S4 (Fig. 1d–g; Extended Data Fig. 4e–k; Supplementary Video 5; Supplementary Table 1). Moreover, the looping neurites form a symmetrical structure along the neuropil's arc, to both demarcate the individual strata and cage all of the strata within the neuropil (Fig. 1g; Extended Data Fig. 4e–h; Supplementary Video 4).

Sensory information streams within neuropil architecture

To understand the functional anatomy of the nerve ring, we first examined axonal positions of the head sensory neurons within the stratified anatomy of the neuropil. There are two main sensory classes of neurons at the anterior buccal tip of the animal: papillary and amphidial sensilla[36]. While these two neuron classes are in close proximity, they are distinguishable by distinct dendritic sensory endings, thought to reflect distinct sensory modalities[36,37]. Both classes of neurons project axons into the neuropil to transduce sensory information onto the nerve ring[36,37]. We found that the papillary axons project to S1 (Fig. 2a–c), while the amphidial axons project to S3/S4 (Fig. 2a,b,d). No papillary or amphidial axons project to S2. Thus, these two distinct sensory organs map onto distinct and specific strata, indicating functional segregation of sensory information and processing within the neuropil's layered structure.

We then correlated circuit-based connectomics[3,14] with the strata organization to reveal additional design principles of neuropil functional organization. Within S1, the papillary sensory cells, which are mechanosensory or polymodal, control head withdrawal reflex behaviors[38]. Most neurons in S1 are part of shallow circuits formed by papillary sensory cells synapsing onto motor neurons (within S1), or even directly onto head muscles[3,38] (Fig. 2e; Extended Data Fig. 3c). Interestingly the S1 circuits retain the symmetry of the papillary sensillum at the interneuron, motor neuron and head neuromuscular synapse level[3,36,37,39]. Topographic maps—the ordered projection of sensory information onto effector systems such as muscles—are a fundamental organizing principle of brain wiring across sensory modalities and organisms[40,41]. We find that S1 displays a topographic map organization, from the primary sensory layer to the motor output representations (Extended Data Fig. 3d–f).

By contrast, amphid sensory axons, associated with plastic behaviors[29,42], innervate S3 and S4. These strata also contain interneurons, but lack motor neurons. Primary and secondary interneurons in S3/S4 synapse upon motor neurons in S1 and S2 (to innervate head and neck muscles) or upon command interneurons in S3 (that connect to motor neurons which innervate body-wall muscles) (Fig. 2e; Extended Data Fig. 3c). Therefore, information streams from the S3/S4 amphid sensory axons segregate to control head/neck muscles (via S1/S2) and body wall muscles (via S3). These findings concur with cell ablation, behavioral, and connectomic studies[16,18,19,43,44], and with anatomical models that the *C. elegans* neuropil is functionally regionalized along the anteroposterior axis[3,18,19]. We note that head exploration (e.g. head withdrawal reflex) or body locomotion (e.g. chemotaxis) behaviors differentially activate distinct motor strategies in response to sensory information[44], consistent with the modular segregation of the sensory information streams now observed for the underlying circuits within the strata. Our observations therefore uncover the somatotropic representations of these behavioral strategies in the architecture of the neuropil, revealing functional design principles in the nerve ring's layered structure, from sensation to motor outputs.

A subset of ‘Rich-club’ interneurons bridge strata

The four neurite strata (S1-S4) account for 151 of the 181 total neurons in the nerve ring (83%). To further understand the nerve ring’s structure, we examined the 30 neurons which clustered differently between the two examined datasets (herein called “unassigned neurons”; Methods). These neurons either a) possessed simple, unbranched processes at boundaries between two adjacent strata (6 neurons); b) had morphologies that cross strata, such as neurite branches projecting into multiple strata, or single neurites that project across strata (21 neurons); or c) showed sparse anatomical segmentations (3 neurons) (Extended Data Fig. 5). Notably, six unassigned neurons were previously placed in the 14-member *C. elegans* “rich-club”[15,20]. Rich clubs are a conserved organizational network property in which highly interconnected hub neurons link segregated modules[15]. The *C. elegans* rich-club comprises 8 command interneurons (including 2 from our unassigned set) and 6 nerve ring interneurons (including 4 from our unassigned set; Extended Data Fig. 5g). Additionally, other neurons from our unassigned set, such as RMG and PVR, are hubs of behavioral circuits[43,45,46].

We examined the unassigned neurons in the context of the strata (Extended Data Fig. 5) by focusing on the ‘rich-club’ interneuron pair of AIBs. The AIB pair was previously shown to morphologically shift between neuronal neighborhoods[3,47], and we found that the morphology, polarity and position of the AIB neurite are precisely arranged to receive inputs from S3/4, and transduce outputs onto S2/3, linking these modular strata. The proximal AIB neurite region lies on the S3/S4 border, while a perpendicular shift of precisely the width of S3 positions the distal region at the S2/S3 border (Fig. 2f–i; Supplementary Video 6). To examine DC output performance, we digitally dissected the AIB neurite into distal and proximal regions and observed, as expected, that the proximal region of AIB specifically clustered with its neighboring S4, while the distal region clustered with its neighboring S2 (Extended Data Fig. 3i–k). We note that AIB’s synapses are similarly partitioned: postsynaptic specializations are primarily in the proximal region in the amphid sensory-rich strata (S3/S4) while presynaptic specializations are localized to the distal region in the motor neuron-rich stratum (S2) (Fig. 2j; Extended Data Fig. 3g,h). This architecture is consistent with AIB’s role in processing amphid-derived sensory stimuli to mediate locomotory strategies[44,48]. Another ‘rich-club’ interneuron pair, AVE, has a similar morphology to AIB: its proximal neurite region borders S2/S3 and its distal region borders S1/S2 (Extended Data Fig. 5a–d; Supplementary Video 7). Neurites of other “rich-club neurons” (RIB and RIA) and “unassigned” neurons (AIZ) similarly shift across the strata (Extended Data Fig. 5a–d,g–u).

Our analyses reveal design principles of the *C. elegans* neuropil at varying degrees of granularity—from single ‘rich-club neuron’ morphologies that functionally bridge different strata, to layered strata that segregate sensory-motor information onto somatotropic representations. These design principles are important organizational units in neuroscience —’rich-clubs’ in the context of brain networks[15,20], laminar organization in the context of brain structures[33,34], and topographical maps in the context of vertebrate sensory systems[40,41].

Layered strata correlate with neuronal cell migrations

To examine the developmental sequence leading to layered nerve ring assembly, we used an integrated platform for long-term, four-dimensional, *in vivo* imaging of embryos. The platform achieves isotropic resolution[7,8,49,50], systematic lineage tracing[9,10], and rendering of cell movements and neuronal outgrowth (represented in the 4D WormGUIDES atlas[51] (https://wormguides.org/; Fig. 3a). The embryonic atlas was systematically examined for birth order, soma positions and lineage identity for all neurons within the strata (Fig. 3b–c; Extended Data Fig. 6). Despite the previous hypothesis that lineage-dependent neuronal soma positions might influence neurite outgrowth into neighborhoods[47], we could not detect any relationships between ancestry or newborn cell position, and the final neurite position within the neuropil strata (Fig. 3b; Extended Data Fig. 6).

Quantification of the positions of individual neurons (belonging to specific strata) in the context of the spatio-temporal dynamics of embryo morphogenesis revealed stereotypic coordinated cell movements that segregated and co-located cell bodies of future S1 stratum. Cell bodies of neurons that later project onto S1 migrated and co-located to the anterior part of the embryo head (anterior to the future neuropil position), while cell bodies of neurons that later project onto S2-S4 migrated to the posterior part of the head (Fig. 3b–d; Extended Data Fig. 7; Supplementary Video 8). For all strata, embryonic soma positions persist until adulthood, and for the future S1 stratum, relate to the cellular morphologies of posteriorly-projecting axonal structures within the anterior stratum of the nerve ring[3,36,37].

In vertebrate embryogenesis, migration of waves of neurons helps organize the layered architecture of the retina and brain cortex[52]. We found that co-segregation of S1 somas in early embryogenesis might serve as an initial organizing principle to define the axes for antero-posterior layering, and later functional segregation of the sensory-motor architecture within the neuropil.

Hierarchical development of the layered neuropil

Previous genetic studies examining nerve ring formation demonstrated roles for glia and centrally located pioneering neurons in its development[21–24]. To build on these findings, we examined neurite outgrowth dynamics during embryonic neuropil formation (Extended Data Fig. 8a–f; Supplementary Video 9). At approximately 390–400 minutes post fertilization (mpf) we observed cells sending projections into the area of the future nerve ring (Fig. 3e,g). Simultaneous use of *mCherry::histone* (to trace these cells' lineage) and ubiquitous membrane-tethered GFP (to observe outgrowth), we identified 6 of these cells as 3 bilateral pairs of neurons: SIAD, SIBV, and SMDD, consistent with pioneering neurons previously identified[21,22] (4 letter name represents a left/right bilateral neuron pair; i.e. SIADL and SIADR, Fig. 3f,h). Additional neurons were observed sending neurite projections alongside these pioneers, but dense ubiquitous membrane labeling prevented us from identifying them via lineaging. To confirm the identities of the 3 lineaged neuron pairs and identify the additional early-outgrowth neurons, we co-labeled embryos with ubiquitous *membrane::GFP* and a cytoplasmic *lim-4p::mCherry* reporter gene (lineaged[51] to express in SIAD, SIBV, and SMDD (Extended Data Fig. 8g–j) and in RIV, SAAV, SIAV, SIBD,

SMDV)). We found all 8 neuron pairs extend neurites into the future neuropil as a tight bundle at 390–400 mpf (Fig. 3i–k; Supplementary Video 10). To further analyze outgrowth timing, we co-labeled embryos with a *pan-neuronal::membrane::GFP* marker and the *lim-4p::mCherry* marker, and observed that these 8 neuron pairs displayed the earliest outgrowth events for the neuropil (Extended Data Fig. 8k–r; Supplementary Video 10,11).

All 8 neuron pairs belong to a neuronal group centrally located in S2 (Fig. 4g–i). To examine the pioneering roles of these neurons in strata formation, we adapted an *in vivo* split-caspase ablation system[53] that ablated these neuron pairs during embryonic neurodevelopment (Extended Data Fig. 8s–x). We then quantified neuropil formation via a *pan-neuronal::membrane::GFP* (Supplementary Video 12). Ablation of the putative 8 pioneering neuron pairs resulted in larval stage 1-arrested animals, and aberrant embryonic neuropils (mean embryonic control vs. ablated neuropil volume was 136.6 μm^3 vs 43.6 μm^3; Fig. 4a–c; Extended Data Fig. 8y,z). Systematic examination of a representative neuron from each stratum (using cell-specific promoters) revealed that putative pioneer neuron ablations affected outgrowth of all examined neurons (Fig. 4d–f; Extended Data Fig. 9). In all cases, neurites paused indefinitely near the positions of the ablated pioneer somas. Thus, embryonic neuropil strata organization appears to be pioneered by a subset of centrally-located S2 neurons.

To understand the pioneers' role in strata formation, we analyzed synchronized recordings of embryonic neurite outgrowth. An ordered sequence of outgrowth events emerged, in which the timing of neurite arrival at the neuropil's dorsal midline correlated with the axial proximity of the examined neurites to the centrally-located pioneer neurites (Fig. 4j; Extended Data Fig. 10a–j'; Supplementary Video 13–15). Our findings extend observations on the hierarchical formation of the neuropil[22], placing the ordered sequence of events within the context of the strata.

Temporal correlation was specific to dorsal midline arrival, but not to initiation of outgrowth from the soma. Notably, S4 neuron AWC was observed initiating outgrowth at 390–400 mpf, similar timing to the pioneering neurons (Fig. 3i; Extended Data Fig. 10k). But instead of entering the nerve ring with the pioneers, AWCs neurites paused for 20.6 minutes (SEM +/− 2.8 min) near the pioneering SAAV somas before entering the nerve ring. (Fig. 3i,j; Extended Data Fig. 10k–s). This pausing point corresponds to the stalling point seen in our pioneer neuron ablation studies (Extended Data Fig. 9c,h,v,y). Thus, while the initial outgrowth events for some neurons occur simultaneously, neurites extend to, and pause at, specific nerve ring entry sites.

The temporal sequence of neurite entries into the nerve ring continues throughout embryogenesis. For example, both the neurites of strata-crossing AIBs, and the looping S1-neurons, outgrow after the neuropil has formed a ring structure (~420 mpf) and after the all the representative neurons of the 4 strata have reach the dorsal midline (~460 mpf). (Fig. 3i–j; Fig. 4j; Extended Data Fig. 10f–j', t–u")[50]. Our observations suggest an inside-out developmental model in which the strata are assembled through timed entry of its components: 1) a pioneering bundle founds centrally located S2, 2) other S2 neurons enter followed by peripherally located S1 (anterior) and S3/S4 (posterior) neurons, 3) followed by

outgrowth of neurons that link the strata, such as the S1 looping neurons or the neurons that cross strata (like AIB).

Lamination is a conserved principle of organization within brains[33,34]. Segregation of functional circuits into layers underpins information processing in sensory systems and higher order structures[35]. In this study we resolve these conserved features of brain organization at a single-cell level and in the context of the nerve ring neuropil, thereby linking fundamental design principles of neuropil organization with the developmental processes that underpin their assembly. Our findings provide a blueprint for synergistic integration of structural connectomic analyses and developmental approaches to systematically understand neuropil organization and development within brains.

Extended Data

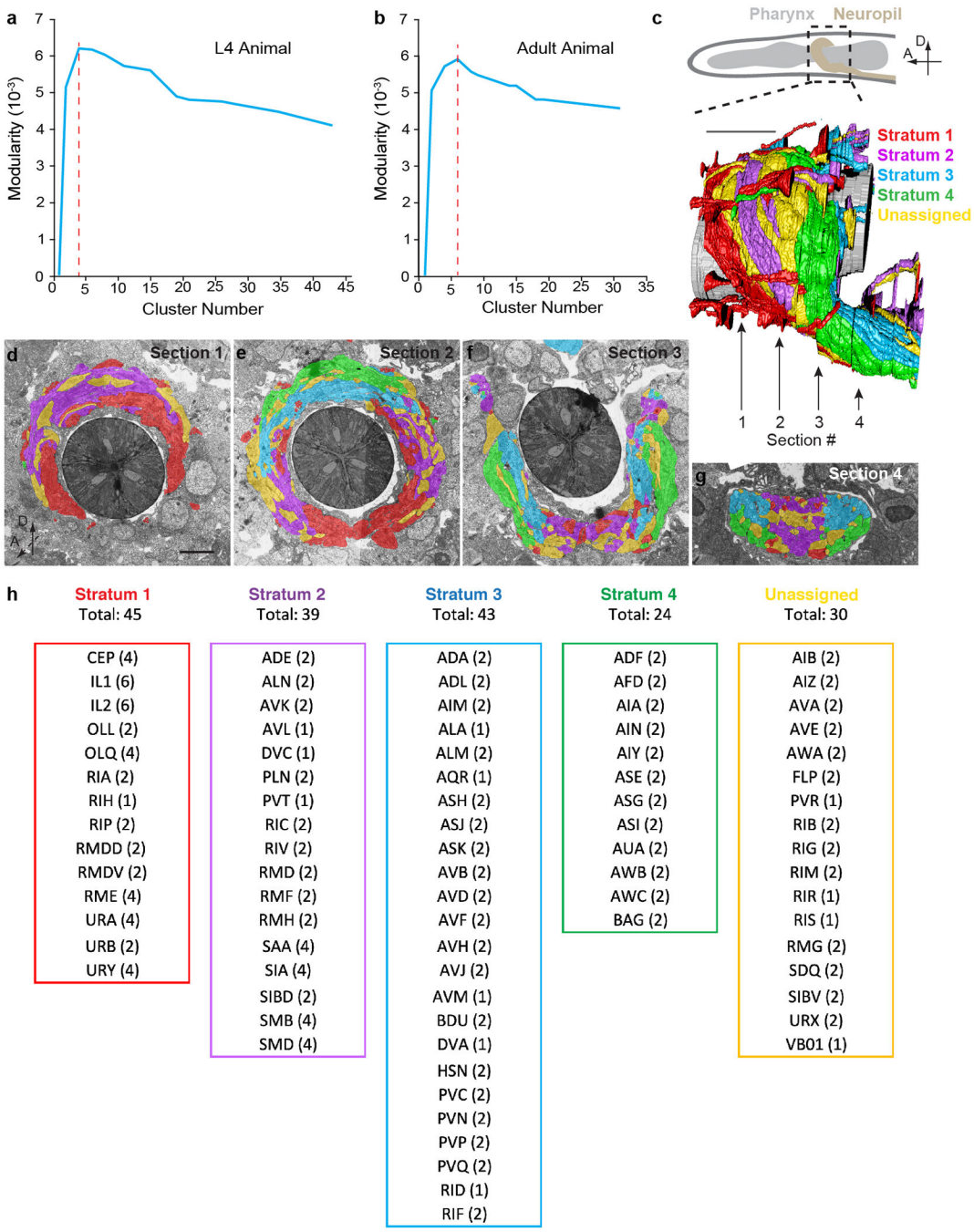

Extended Data Figure 1. DC analyses of the nerve ring neuropil.

a-b, Quantification of network modularity[32,55] for DC analysis of L4 (**a**) and adult (**b**) animal. DC iteratively groups neurons based on quantitative similarities of each neurons' contact profile, unveiling data relationships at varying scalers of granularity (Fig. 1b). We calculated network modularity for each iteration. Note that the highest modularity score was for the iteration with four clusters (in the L4 stage animal) and 6 clusters (in the adult animal). Comparisons revealed that for the adult animal, there were four large clusters

similar to the L4 stage animal, and two smaller ones (see Methods; Extended Data Fig. 2a–d). Some of these neurons from the two smaller clusters in the adult also clustered in the L4 animal, but in an earlier iteration (Extended Data Fig. 2m–n). The iterations with the highest modularity scores were then used for subsequent strata analyses in the manuscript (see Methods), but we emphasize that other iterations reveal other valuable data relationships at varying scale of granularity, including cell-cell and circuit-circuit interactions (Extended Data Fig. 3a–b). **c,** Volumetric reconstruction of the L4 stage *C. elegans* neuropil (from EM serial sections[3]) with the 4 strata and unassigned neurons individually colored. Above, schematic of worm head with nerve ring neuropil (dashed box). Location of EM sections displayed in (**d-g**) shown below (arrows and corresponding section numbering). Scale bar is 5 μm. **d-g,** Segmented serial section electron micrographs from[3], neurons colored as in (**c**). Original EM slices 41, 92, 152, 206 shown in **(d-g)** respectively. Scale bar (2.5 μm, in **d**) applies to panels (**d-g**). **h,** Listing of neuronal classes in the 4 strata, and the 'unassigned' group. Number to the right of each neuron represents total neurons for each class, for all 181 neurons in the nerve ring neuropil.

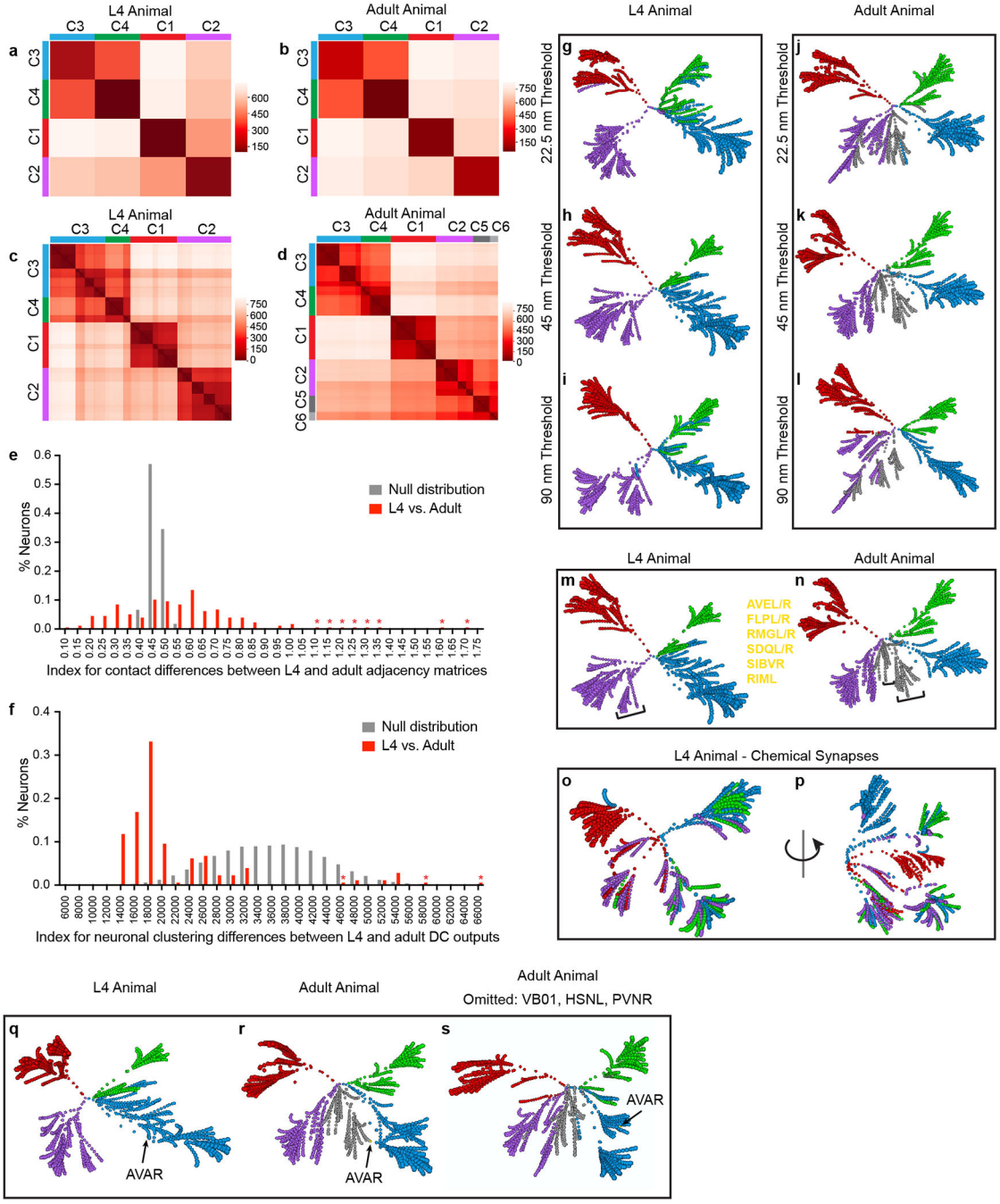

Extended Data Figure 2. Analyses of the L4 and adult contact adjacency matrices, DC outputs, and C-PHATE plots.

a-b, Heatmap of scaled neuron distances within the DC nested hierarchy outputs for the L4 (**a**) and adult animal (**b**). Values were calculated by measuring all distances between neurons from 1 cluster to another cluster and then averaged (see Methods). This was done for the clusters at the iteration with the highest modularity score (see Fig. 1b and Extended Data Fig. 1a–b). The two smaller clusters from the adult were excluded. Coloring scale displayed to the right of the heatmap. Darker colors indicate smaller average

distance. Note how C3 is closer to C4 and C1 is closer to C2 in distance. **c-d,** As (a-b) except scaled distance values were calculated by measuring the distances between every neuron within the DC output. Two additional clusters in the adult are colored grey. Note varying scales of granularity in neuronal relationships that constitute the major clusters, and, similar to the C-Phate plots, circuits such as thermotaxis and body mechanosensation can be found in the more granular areas (see Extended Data Fig. 3a–b). **e,** Histogram of the distribution of contact profile differences for each neuron between the L4 and adult contact adjacency matrices. Briefly, we calculated an Index of Difference (see "Contact Adjacency Data Analysis" in Methods) for each neuron, comparing the contact profiles of the adult and L4 animals. We also generated 2004 random adjacency matrices to simulate distributions of random contact profile differences. We determined that the contact profiles of 49/178 neurons (28%) were significantly more similar than random ($p<.05$), whereas the contact profiles of 96/178 neurons (54%) were significantly more different ($p<.05$; by unpaired two-tailed Student's t test between L4 vs. Adult and Null Distribution; df= 178532, no adjustments were made for multiple comparisons; see Methods). Therefore, there are a substantial portion of neurons that have statistically different contact profiles between L4 and adult. Additionally, we calculated the Jaccard distance and found that the average neuron's contact partner list was 37.6% different between the L4 and adult animal, consistent with previous analysis[18]. As further discussed in "Supplementary Discussion 3", we believe differences between the contact profiles in the connectomes could be due to a large number of small, varying contacts. In the graph, a higher index number reflects a neuron with a higher amount of contact differences between L4 and adult. Red bars represent the differences between L4 and adult (178 neurons in total). Grey bars are the null difference distribution. Asterisks denote the location of single neurons that are hard to see on the graph. **f,** same as in (e) except for histogram represents distribution of differences in neuronal distances within the DC hierarchical outputs (See "Diffusion Condensation Data Analysis" in Methods). Interestingly, we found that, unlike the contact adjacency data, the DC output clustering location was significantly similar in 127/178 neurons (71%) ($p<.05$), whereas only 9/178 neurons (5%) were significantly different than random ($p<.05$; by unpaired two-tailed Student's t test between L4 vs. Adult and Null Distribution; df= 881276, no adjustments were made for multiple comparisons; Methods). These analyses, in the context of the differences seen for the contact profiles (**e**), indicate that the DC algorithm identifies meaningful relationship within the neuropil tangled and varying contact profiles. **g-i,** C-PHATE plots of DC analyses preformed on adjacency matrices calculated using different contact thresholds for the L4 animal. Data presented in Fig. 1b was calculated with the 45 nm threshold. 45 nm is approximately 10 pixels in the EM datasets. DC correctly defines clusters even for the different thresholds. **j-l,** same as in (**g-i**) except for the adult animal. **m-n,** C-PHATE plots of the L4 and adult animal. The adult animal has 2 additional clusters at the highest modularity score. These clusters (shown in grey) are composed primary of neurons that interact across multiple strata. Additionally, neurons from these smaller clusters in the adult also co-clustered in the L4 animal, but at an earlier iteration. Brackets indicate location of the cluster in the L4 and adult that is composed of similar neurons. The neurons within the cluster are listed between the two plots. **o-p,** C-PHATE plot of DC analyses preformed on the chemical synaptic connectomics data from the L4 animal (wormwiring.org). Note that the C1 cluster, and part of the C3 cluster, are similar

between the connectomic and contact DC analysis outputs. However, C2/C3/C4 are mixed in the connectomics DC output. (p) is a rotation of (o) to show the partially retained C3 blue cluster, as seen at the top of the graph. Interestingly, we also found that the neuropil pioneers (Fig. 3i–k) that cluster in C2 in the contact DC analysis are now scattered among the different mixed clusters in the connectome DC analysis. The pioneering neurons SIA and SIB make almost no presynaptic contacts and very few postsynaptic contacts. This dispersion of the pioneers among different clusters in the connectome DC analysis highlights the value of using contact analysis to uncover the structural architecture of the neuropil, especially for neurons that are synaptically sparse. **q-s,** C-Phate plots for the L4 animal (g), adult animal (h), and the adult animal where the neurons VB01 (and also HSNL and PVNR) were omitted from the adjacency matrices used to calculate the DC/C-Phate plot (i). These are the only 3 neurons that are exclusively found in the adult because they haven't grown into the neuropil at the L4 stage. We observed that AVAR (C-Phate plot location annotated with arrows) is assigned to Cluster 3 in the L4 animal and to Cluster 5 in the adult animal. AVAR makes extensive contact with VB01 in the adult animal that are absent in L4 animal. We eliminated the VB01 neuron profile and contacts from the adult dataset and, consistent with our analyses, observed that AVAR now similarly clustered, as in the L4 dataset, to Cluster 3 in the adult dataset lacking VB01. This demonstrates that developmental differences affecting the contact profile of neurons leads to differences in the DC outputs between the L4 and adult animals. Note that AVAR does not contact the other two neurons that were omitted in these analyses (HSNL and PVNR); suggesting that omission of VB01 is causative for the change in AVAR clustering. Graphs or plots in (a,c,g-i,m,o-p,q) colored according to the 4 clusters identified in iteration 23 of the L4 animal as in (Fig. 1b) using the 45 nm threshold: C1-Red, C2-Purple, C3-Blue, C4-Green. Graphs or plots in (b,d,j-l,n,r-s) colored according to the 6 clusters identified in iteration 22 of the adult animal using the 45 nm threshold: C1-Red, C2-Purple, C3-Blue, C4-Green; C5/6-Grey).

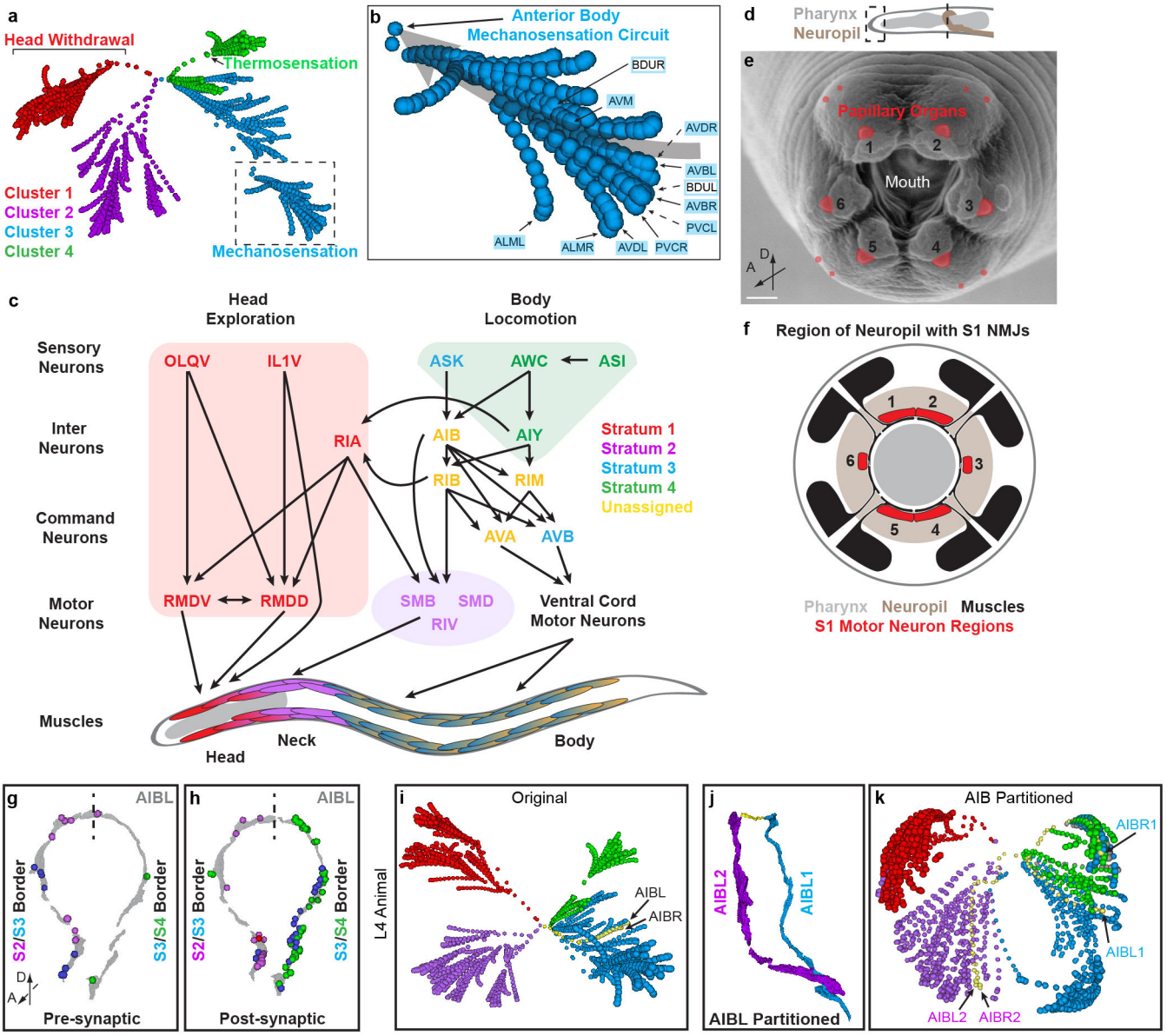

Extended Data Figure 3. Examination of behavioral circuits in the DC/C-PHATE analyses

a, C-PHATE plot of DC analyses for a larval stage 4 (L4) animal, with known behavioral circuit locations highlighted. **b,** Enlargement of inset from (**a**) displaying the condensation of a group of neurons corresponding to the mechanosensation circuit [30,43,56,57]. Neurons with their names in filled blue boxes are members of the anterior body mechanosensation circuit, neurons with their names in outlined blue boxes (BDUL and BDUR) have been proposed to guide the formation of the circuit during development[57]. **c,** Model of functional segregation of information streams within the neuropil. Papillary sensory information is processed in S1 and innervates head muscles to control head movement. Amphid sensory information is processed in S3/S4 and links to body muscles (via command interneurons) and neck muscles (via motor neurons in S1/S2) to control body locomotion[29,38,42,58]. Interneurons cross strata to functionally link these modular circuits (Extended Data Fig. 5). Individual

neuron classes and muscle outputs are colored according to the strata they belong to (for muscles, according to the strata the innervating neurons belong to). **d,** Schematic of *C. elegans* head highlighting area in (**e-f**) as dashed rectangle and line, respectively. **e,** Representation of S1 sensory organs, projected over a scanning EM of the *C. elegans* mouth. Numbers highlight the 6-fold symmetry of the papillary organs. Image produced by and used with permission of David Hall. Mouth sensilla colored according to their strata assignment. Scale bar is 1 μm. Same image as Fig. 2b. **f,** Topographical map of the S1 shallow head circuit. The S1 motor neurons, which have a "4-fold-plus-two" symmetric pattern[39], make neuromuscular junctions (NMJs), projecting their symmetry onto the 4-fold symmetrical muscle quadrants that control head movement (black)[39] (compare to (**e**) above, see also[39]). Numbers represent the four-fold-plus-two symmetry of the S1 neurons in (**e**). Briefly, for example, for IL1 neurons, the dorsal and ventral IL1 neuron pairs (in our schematic, 1,2 and 4,5) connect to the dorsal and ventral muscle octants, while the lateral IL1 neurons connect to the two lateral muscle octants (in our schematic, 6 and 3 represent the two lateral IL1 neurons)[39]. **g-h,** Axial view of the 'rich-club' AIB left (AIBL) interneuron[15,20] (Fig. 2f) with distribution of the presynaptic (**g**) and postsynaptic (**h**) sites colored according to the strata of the corresponding AIBL synaptic partner. Vertical dashed line indicates division between proximal and distal regions of the neurite. Similar distribution was seen for AIB right (AIBR, not shown). **i,** C-PHATE plot of DC analysis for the larval stage 4 (L4) animal. AIBL/R are colored yellow to highlight their location within the plot. **j**, Volumetric reconstruction of the unassigned (yellow), 'rich-club' AIBL interneurons[15,20] depicting the regions of AIB that were partitioned in the EM data. Proximal region in blue (AIBL1), lateral region in yellow, distal region in purple (AIBL2). AIB's proximal region borders S3/S4, and the distal region borders S2/S3 (Fig 2. f–i). **k**, C-PHATE plot of DC analysis for the larval stage 4 (L4) animal after AIB's had been partitioned in the EM dataset. AIB1s and AIB2s are yellow and the AIB lateral regions seen in (**j**) are grey. Note how after partitioning the proximal regions (AIB1s) remains within C4, while the distal regions (AIB2s) now cluster with C2, demonstrating that DC/C-PHATE analysis clusters neurons based upon their neighboring contact profiles. Plots in (**a,b,i-k**) colored according to the 4 clusters identified in iteration 23 of the L4 animal as in (Fig. 1b): C1-Red, C2-Purple, C3-Blue, C4-Green.

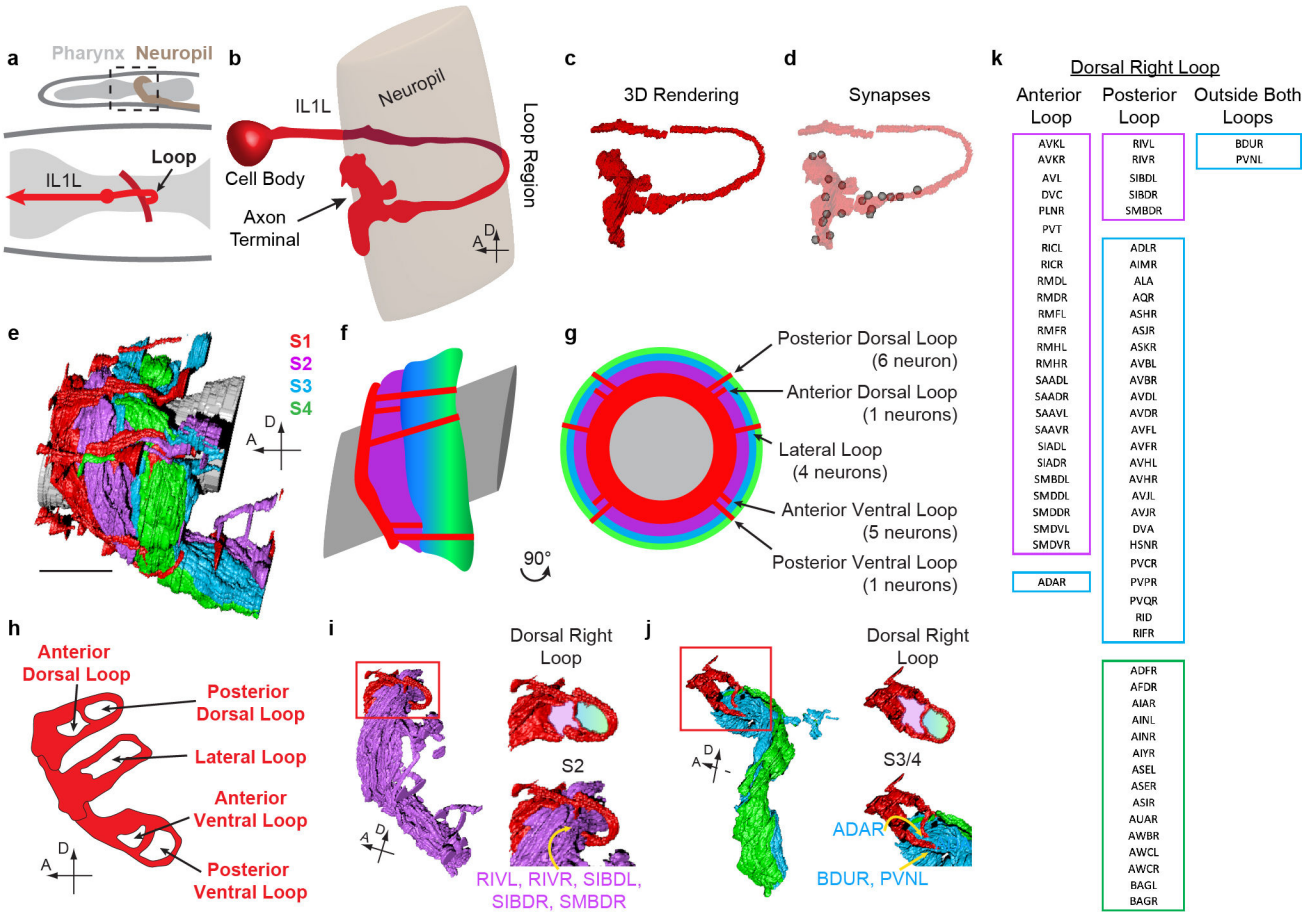

Extended Data Figure 4. S1 structure precisely encases S2, S3, and S4 of the neuropil

a, Illustration of the IL1L neuron based on data presented in "Mind of the Worm"[3] (additional information available at wormatlas.org). Schematic of worm head and neuropil (dashed box) above. In schematic below, IL1 neuron in red, with dendrite (left pointing arrow), soma (circle) and axon (right pointing loop, arrow). Pharynx (shaded gray) for reference. **b**, Cartoon of IL1L loop in the context of the nerve ring neuropil (sensory dendrite not show). **c**, Volumetric reconstruction of IL1L from L4 animal EMs. **d**, Overlay of IL1L volumetric reconstruction and synapses (grey spheres) highlighting the position of the synaptic endplate (after the neuron loops around the neuropil). **e,** Volumetric reconstruction of the L4 neuropil with individual neurons from the 4 strata colored (S1-Red, S2-Purple, S3-Blue, S4-Green). Scale bar is 5 μm. **f-g**, Schematic of the structure formed by the S1 looping structures, from a lateral (**f**) and axial (**g**) view with neuropil strata. **h**, Schematic of the S1 loops (lateral view) without the strata (as Fig. 1d) **i-j,** Volumetric reconstruction of Dorsal Right Loop and S2 (**i**) and S3/S4 (**j**) with individual neurons that fall outside of the looping structure rule (yellow arrows). Although 90% of S2, 84% of S3 and 100% of S4 neurons are contained within the indicated loops, a minority of neurons belonging to S2 and S3 strata are not encased by the loops corresponding to the specific strata. We include the names of these neurons below the volumetric reconstructions; Supplementary Video 5. **k,** List of all neurons and their positions in the dorsal right loop structures, colored according to the 4 strata (a complete listing of all neurons, and their

positions within the 6-fold symmetric honeycomb structure, can be found in Supplementary Table 1, and movie projections of the honeycomb-like structure in the context of the strata in Supplementary Videos 4–5).

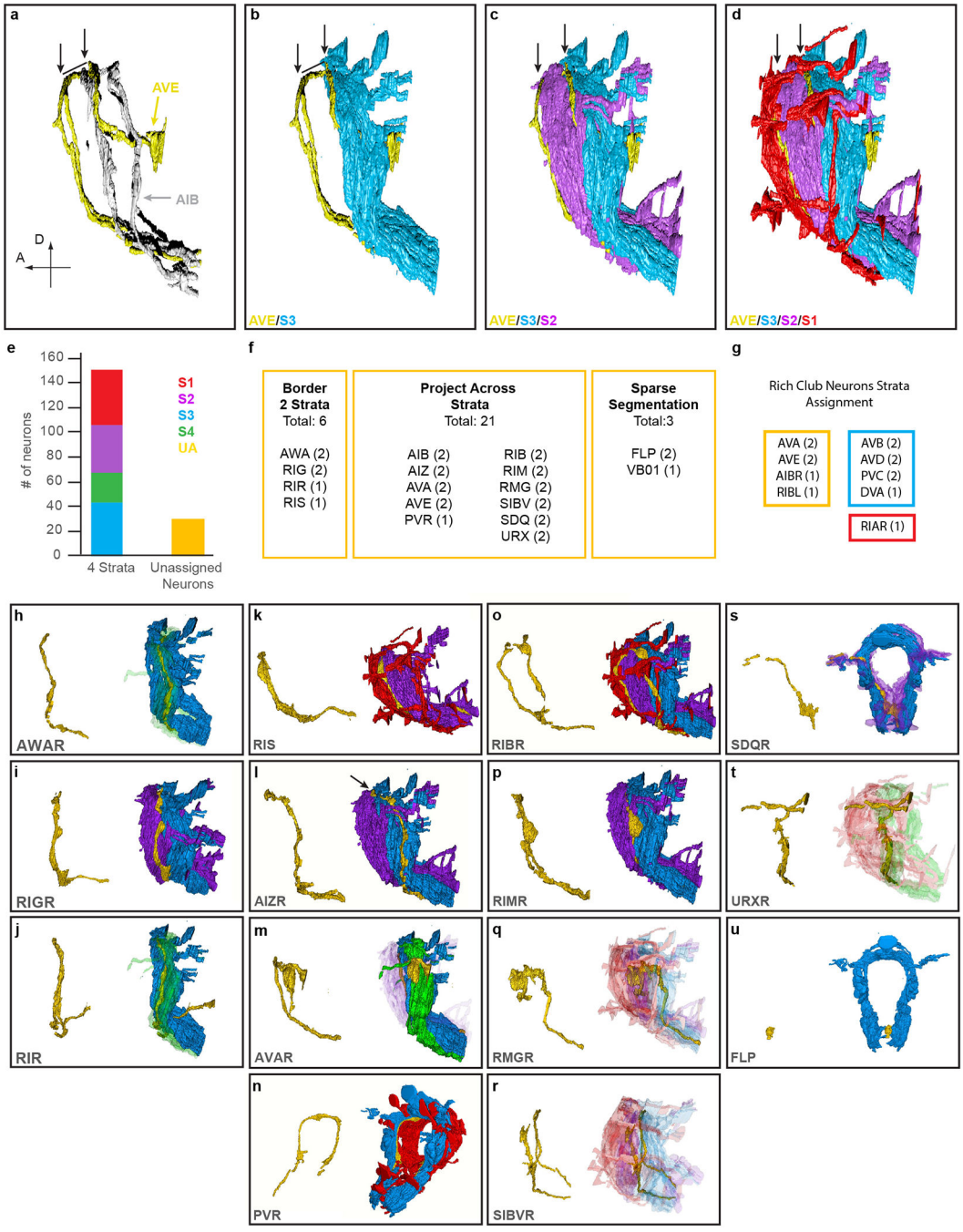

Extended Data Figure 5. Neurons unassigned to the 4 strata anatomically contact multiple strata and a subset belong to the highly interconnected "rich-club" neurons.

a-d, Volumetric reconstructions of the unassigned AVE interneuron (yellow) in the context of nerve ring strata, with AIB (grey). Arrows indicate the two segments of AVE that border strata. AVE has a similar morphology to AIB (Fig. 2f) but is anteriorly displaced by one

stratum: AVE borders S2/S3 (**b-c**), shifts along the A-P axis, and then borders S1/S2 (**c-d**). Lines in (**a,b**) indicates AVE shift along the A-P axis to shift strata; Supplementary Video 7. **e,** Analysis of the total number of neurons within each stratum, and in the unassigned group. **f,** Classification of 'unassigned' neurons. **g,** Stratum location of the rich club neurons[15,20]. Colored box depicts strata assignment. These 14 neurons functionally consist of two groups: 8 command interneurons (which modulate the backward and forward locomotion; AVA, AVB, AVD, PVC) and six nerve ring interneurons (AVE, AIBR, RIBL, RIAR, DVA). The six command interneurons that are not part of the unassigned group have neurites that remain within S2. The 2 command interneurons that are part of our unassigned group (AVA) border S2 and S3, and contain a large protrusion that crosses S3/S4 (see Extended Data Fig. 5m). Of the 6 "rich club" interneurons, four of them were identified in our DC analyses as neurons that cross strata. One that was not identified in our analysis is RIAR, but it is a neuron that also crosses between S1 and S4. As such our study extends the understanding of the rich club interneurons in the context of the nerve ring, particularly the subgroup of rich club interneurons which are not part of the command interneurons. **h-u,** Volumetric reconstructions of all unassigned neurons highlighting their strata interactions. **h,** AWA borders S3/S4. **i,** RIG borders S2/S3. **j,** RIR borders S3/S4. **k,** RIS borders S1/S2. **l,** AIZ shifts perpendicularly from S3 to the S2/S3 border, highlighted with arrow. **m,** AVA borders S2/S3 and protrudes into S3 and S4. **n,** PVR borders S1/S3 and protrudes into S1. **o,** RIB forms a cage-like structure around S2. **p,** RIM borders S2/S3 and protrudes into S3. **q,** RMG protrudes into S1/S2/S3. **r,** SIBV's main neurite is in S2, but it sends a second neurite into S1. **s,** SDQ borders S2/S3. **t,** URX interacts with S1 and S4. **u,** FLP has sparse segmentation data in the nerve ring. Images are rotated relative to each other, and transparency settings vary between images, for clarity in display of their position within the nerve ring. Neurons arranged according to (**f**).

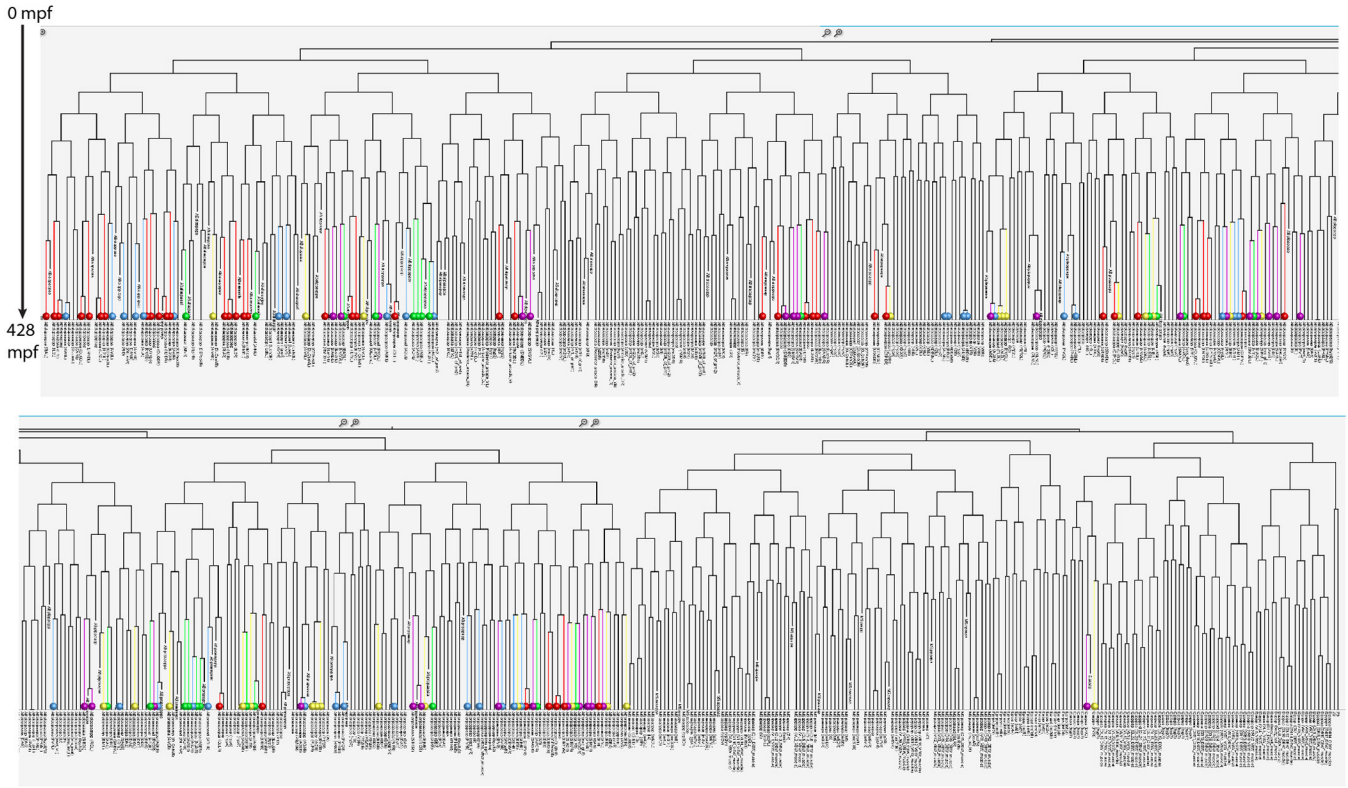

Extended Data Figure 6. Analysis of the 4 strata in the context of the lineage tree

a, Lineage tree for *C. elegans* (0–428 minutes post fertilization). Each neuron's terminal branch is colored according to its stratum assignment and marked with a similarly colored sphere. Lower panel is part of the lineage tree above. Upon detailed examination of all 181 neuropil neurons in the context of the lineage tree, while we observe clusters of neurons, we could not systematically correlate those clusters (representative of terminal lineage positions) with stratum assignment. This image was generated using WormGUIDES[51]. For access to a fully interactive lineage tree see Supplementary Discussion 1.

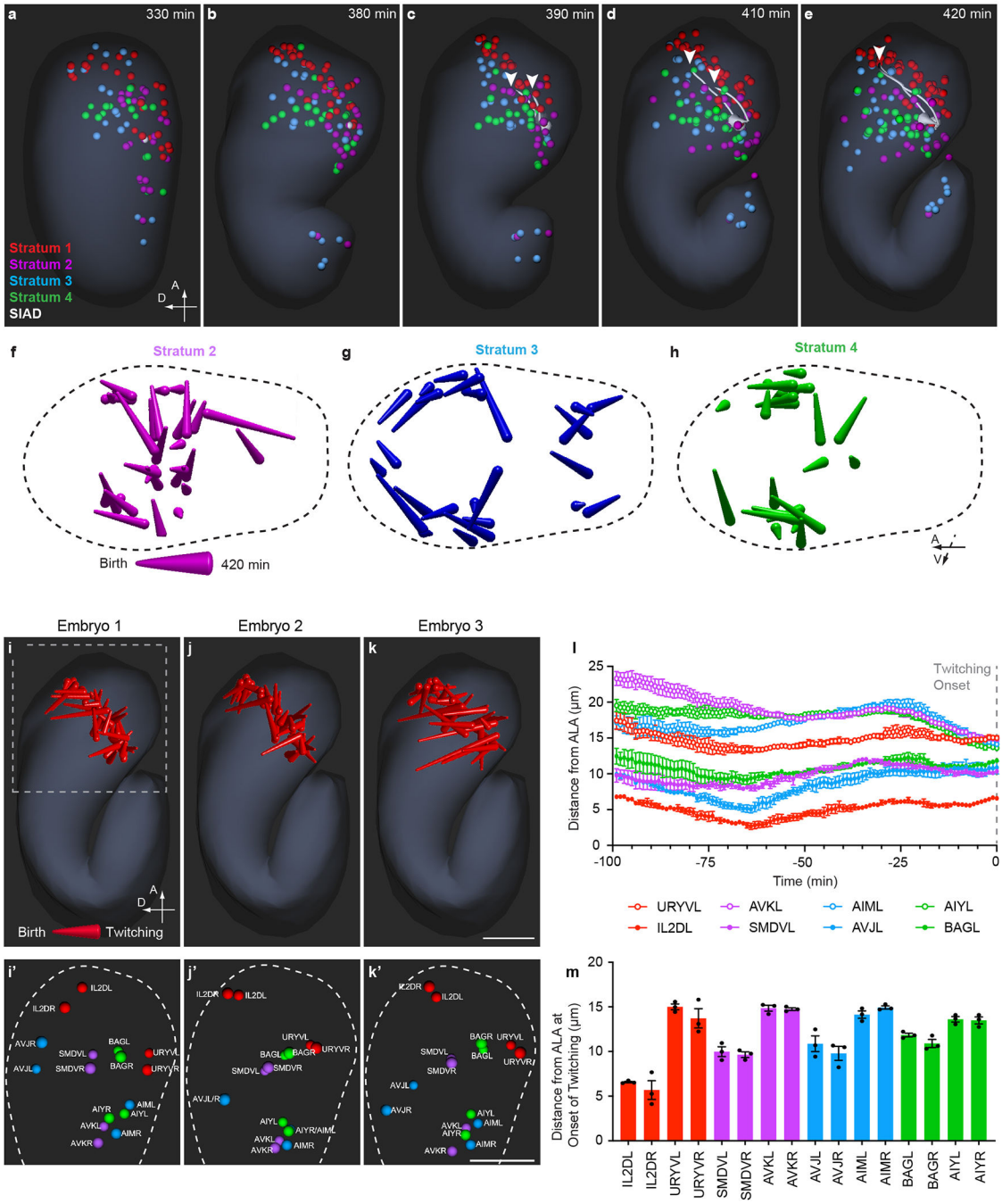

Extended Data Figure 7. Early stereotypic segregation of neuronal somas correlates with neuropil strata architecture.

a-e, Time series of neuronal soma positions within the embryo (generated using WormGUIDES[51]). We analyzed soma positions from ~70 to 430 mp; during this interval the embryo proceeds through gastrulation, into the early stages of elongation, and the majority of the terminal neuronal cell divisions are completed. We found that soma segregation occurs between 330–420 mpf. S2 pioneer neuron, SIAD, in white for reference of nerve ring position. White arrowheads in (**c,d**) highlight the growing tips of the pioneer SIAD. White

arrowhead in (**e**) highlights the dorsal midline (meeting point for the bilateral SIADs). Note that S1 somas are anteriorly segregated prior to pioneer neurite outgrowth (Supplementary Video 8). **f-h,** 3D depth trajectories displaying the movement of cells that will extend their neurites to S2 (**f**), S3 (**g**) or S4 (**h**) (movement represented from neuronal cell birth to 420 mpf). S2 movement has a ventral bias. S3 movement is principally along the outermost embryonic edge, and S4 clusters into 2 bilaterally symmetric groups. **i-k,** 3D depth trajectories of S1-cell movements between neuronal cell birth and 420 mpf for 3 different lineaged embryos. Embryo in (**i**) is the same dataset as embryo shown in (**a-h**) and in Fig. 3b–d. The migration trajectories for all 3 embryos is stereotypic. Dashed box highlights area shown in (**i'-k'**). Scale bar (10 μm) applies to panels (**i-k**). **i'-k',** Neuronal soma positions for cells from the four strata just before twitching onset. Same embryos as in (**i-k**). Similar to the migration trajectories (**i-k**) the positions of neuronal somas from each stratum are stereotypic across individuals. Scale bar (10 μm) applies to panels (**i'-k'**). **l,** Quantifications of average 3D distances from selected neuronal somas to the ALA neuron soma over a 100 min. interval up to the start of twitching (430 mpf). ALA was used as reference because its position was reported to be reproducible between individual embryos[59]. The migration paths for neurons from the 4 strata are stereotypical across animals, and we found that the average neuron's 3D distance from ALA varies by a standard deviation of less than a micron (~0.73 μm). **m**, Quantification of average 3D distances from selected neuronal somas to the ALA neuron soma just prior to onset of twitching (430 mpf). Neuron somas in all panels colored according to strata assignment (S1-Red, S2-Purple, S3-Blue, S4-Green). For (**l-m**) means are from 3 embryos (same embryos as in (**i-k'**). All error bars are mean +/− SEM.

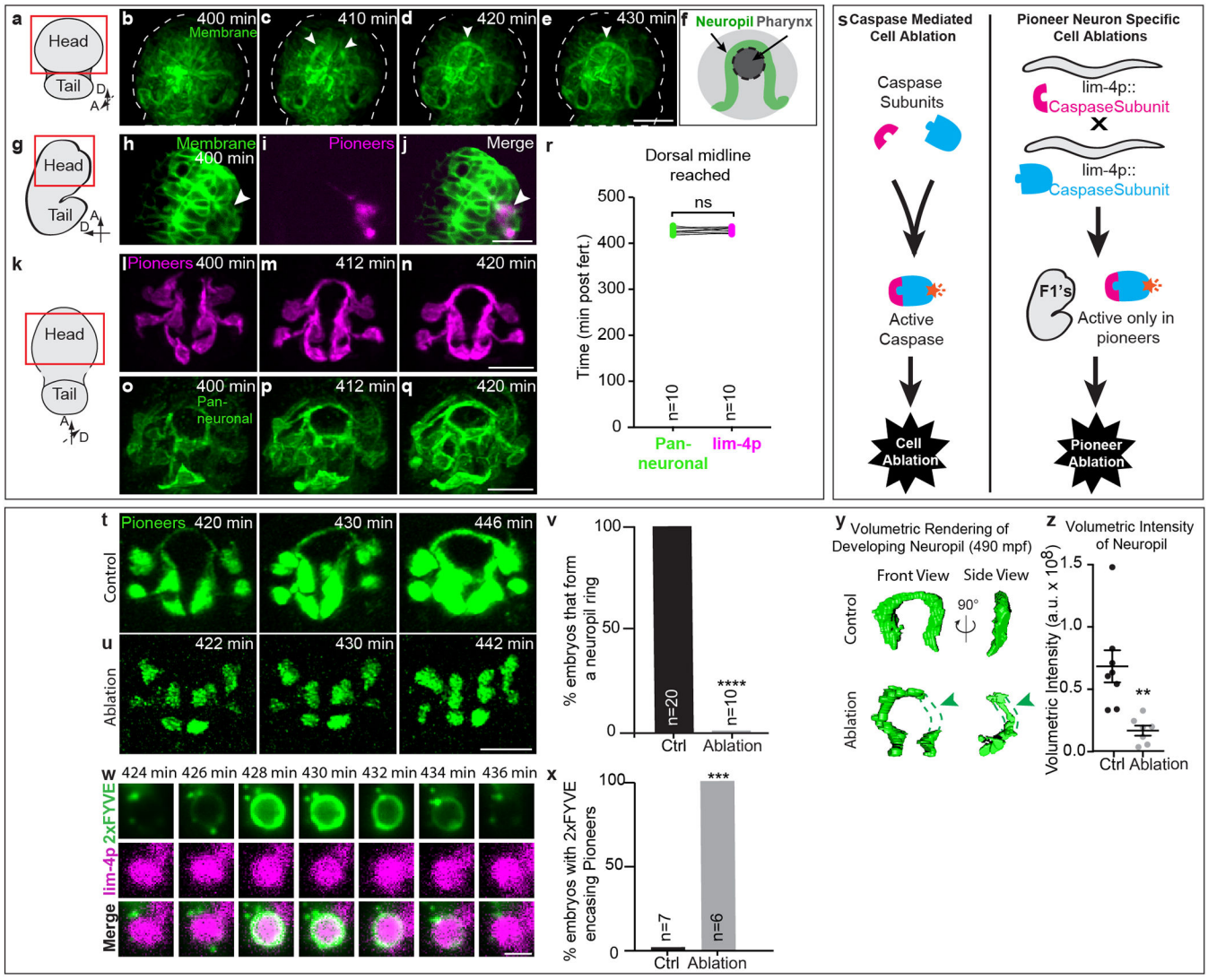

Extended Data Figure 8. S2 pioneering neurons outgrowth initiate development of the stratified neuropil and are required for nerve ring neuropil development.

a, Schematic of *C. elegans* embryo depicting region displayed in (**b-f**), red box. **b-f**, Time-lapse of the outgrowth dynamics of the neuropil (labeled with ubiquitous *nhr-2p::membrane-tethered::GFP*) and schematic. Arrowheads indicate first extensions entering the future neuropil. Deconvolved diSPIM maximum intensity projections are shown (n=8 embryos; Supplementary Video 9). **g,** Schematic of *C. elegans* embryo depicting region displayed in (**h-j**), red box. **h-j**, Comma stage embryo (400 mpf) co-labeled with ubiquitous (*nhr-2p::membrane-tethered::GFP*) and pioneer neuron (*lim-4p::mCherry*) markers. Membrane and pioneer expression co-localize in SIAD, SIBV, and SMDD confirming the lineaging analysis (see Fig. 3e–h). Single z-slice acquired with a single diSPIM arm shown (n=12 embryos). Arrow indicates co-labeling of the two markers. **k,** Schematic of *C. elegans* embryo depicting region displayed in (**l-n,o-q**), red box. **l-n**, Time-lapse of the outgrowth dynamics of pioneer neurons (labeled with *lim-4p::membrane-tethered::GFP*). The same image series was used in Fig. 3i,j and are displayed here for

comparison with the next panels. Deconvolved diSPIM maximum intensity projections are shown (n=16 embryos). **o-q**, Time-lapse of the outgrowth dynamics of the neuropil (labeled with *rab-3p::membrane-tethered::GFP*). Deconvolved diSPIM maximum intensity projections are shown (n=3 embryos). Neuronal outgrowth into the neuropil occurs simultaneously for pioneers (**l-n**) and the first pan-neuronal outgrowth events detected (**o-q**), suggesting the S2 pioneers are the first to enter the developing neuropil (Supplementary Video 11). **r,** Analysis of timing for arrival to the dorsal midline in a strain co-labeled with *rab-3p::membrane-tethered::GFP*, and *lim-4p::mCherry*. Points connected with a line correspond to datapoints from the same embryo (n=10 embryos). "ns" not significant by paired two-tailed Student's t test. **s,** Schematic of caspase ablation strategy for pioneer neurons. Left panel depicts split-caspase induced cell ablation, as described in[53]. Right panel depicts pioneer-specific split-caspase ablation assay in embryos. The *lim-4p* promoter was used to drive caspase expression in the SIA, SIB, SMD, RIV, and SAAV neurons, ablating them prior to neurite outgrowth. F1 is first generation after mating. **t-u,** Time-lapse of the outgrowth dynamics of the pioneering neurons in control (**t**) and pioneer ablated (**u**) embryos (labeled with *lim-4p::mCherry*). Pixel intensities are different for (**t,u**) due to significant decrease in signal in the ablated animals. Deconvolved diSPIM maximum intensity projections are shown (Ctrl n=20 embryos; Ablation n=10 embryos). Previous studies showed that laser-ablations of subsets of these pioneer neurons were wild-type[60], suggesting existence of functional redundancy in guiding nerve ring development. **v,** Quantification of the percentage of embryos forming a full neuropil ring in control and pioneer-ablation embryos. n= number of embryos scored. ****p<0.0001 by two-sided Fisher's exact test between Ctrl and Ablation. **w,** Time-lapse of the dynamics of 2xFYVE on ablated pioneering neuron somas. 2xFYVE is a marker of cell death and appears around cell corpses as described[54]. To see cell corpses of pioneer neurons, embryos were labeled with *ced-1p::2xFYVE::GFP(S65C,Q80R)* (to image cell corpses) and *lim-4p::mCherry* (to image pioneer neurons). Single Z-plane from diSPIM dataset shown (Ctrl n=7 embryos; Ablation n=6 embryos). **x,** Quantification of 2xFYVE encasing ablated pioneer somas. ***p=0.0006 by two-sided Fisher's exact test between Ctrl and Ablation. n= number of embryos scored. **y,** Volumetric reconstruction of the developing neuropil for control and pioneer ablated embryos. Volumes were acquired from diSPIM images analyzed with 3D Object Counter (FIJI-ImageJ2; Methods). Green arrowheads emphasize aberrant neuropil phenotypes in ablation animals (gaps in the neuropil and decreased widths). **z,** Analysis of pixel intensity within the neuropil volume of control and pioneer ablated embryos. Each dot represents the summation of all pixels within a neuropil volume for 1 embryo (Ctrl n=8; Ablation n=7), quantified using 3D Object Counter (FIJI-ImageJ2; Methods). **p=0.0032 by two-tailed Student's t test between Ctrl and Ablation. Error bars are mean +/− SEM. Timing for all panels is mpf. Scale bar (10 μm) applies to panels in corresponding sections (**b-e, h-j, l-n, o-q, t-u**); Scale bar (3 μm) applies to panels in (**w**).

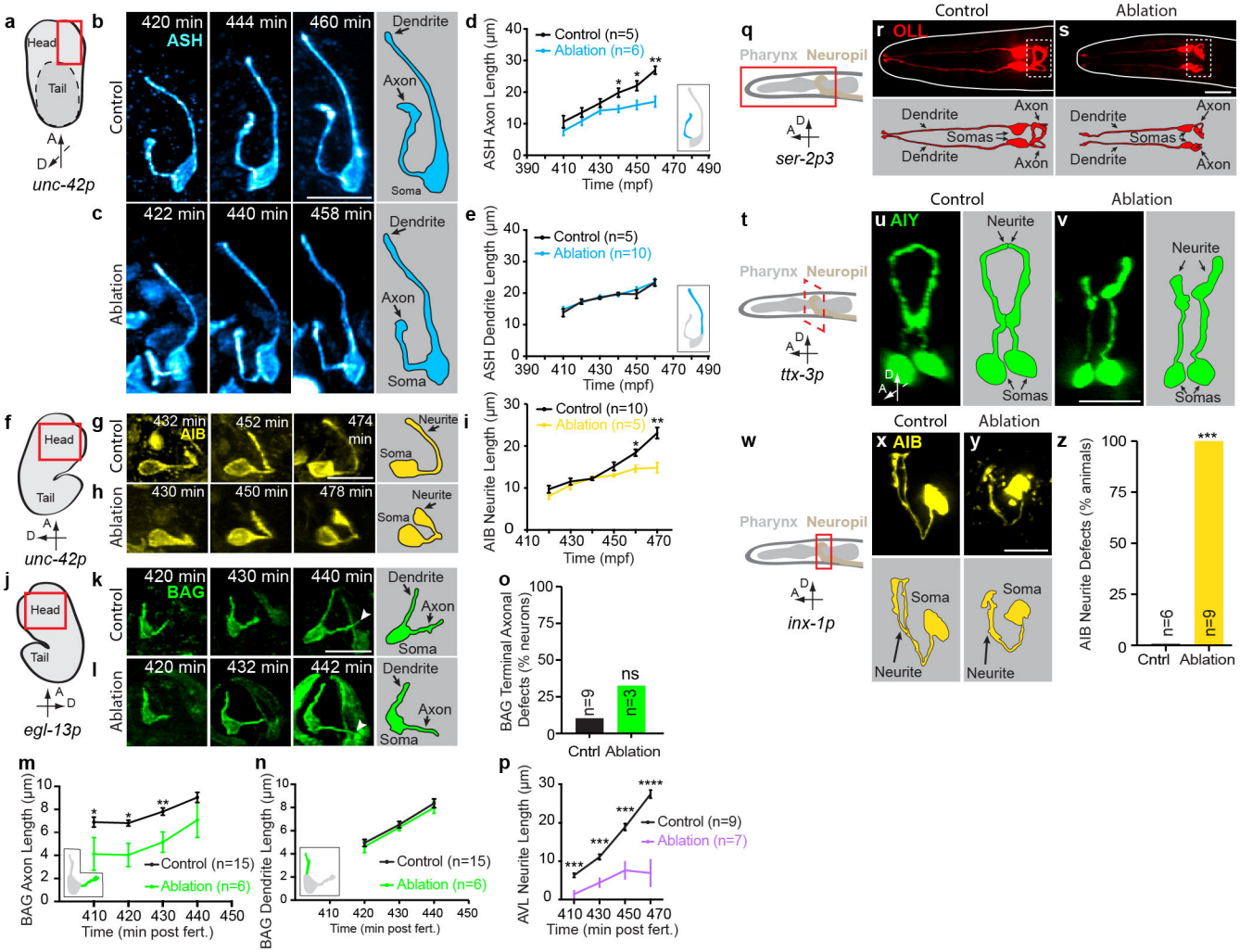

Extended Data Figure 9. S2 Pioneer neurons are required for the development of neurons from all 4 strata, and the unassigned neurons.

a, Schematic of embryo, highlighting area in (**b-c**) as red rectangle. Promoters used are shown below schematic in italics. **b-c,** Time-lapse of outgrowth dynamics of Stratum 3 neuron ASH in control (**b**) and pioneer ablated (**c**) embryos, with schematic (right hand side). Deconvolved diSPIM maximum intensity projections shown (Ctrl n=5 neurons; Ablation n=6 neurons; Supplementary Video 14). **d-e,** Quantifications of ASH axon (**d**) or dendrite (**e**) outgrowth for control and ablated animals. Note how axons (which are in the nerve ring) are affected by nerve ring pioneer neuron ablations, while dendrites (which are not in the nerve ring) are not affected. 'n' = number of neurons quantified. *p<0.05, **p<0.01, ***p<0.001, ****p<0.0001 by unpaired two-tailed Student's t test between Ctrl and Ablation at each timepoint (see Methods for exact p-values). Timepoints without annotation are "ns" (not significant). Error bars are mean +/− SEM. **f-i**, As for (**a-d**), but for unassigned interneuron AIB (Ctrl n=10 neurons; Ablation n=5 neurons; Supplementary Video 15). **j-n,** As for (**a-e**), but for S4 neuron BAG (Ctrl n=15 neurons; Ablation n=6 neurons;). **o**, Quantification of the percentage of BAG neurons with defective morphologies at 444 mpf for control and pioneer ablated animals. Note that BAG neurons are delayed

in early outgrowth, but eventually find their terminal locations, suggesting guidance of this neuron relies on redundant mechanisms. ‘n’ = number of embryos. “ns” not significant by two-sided Fisher’s exact test between Ctrl and Ablation. **p,** As for (**d**) but for S2 neuron AVL shown in (Fig. 4d,e). **q,** Schematic of *C. elegans* head highlighting area in (**r-s**) as red rectangle. **r-s**, Larval stage 1 (L1) images of S1 neuron OLL in control and pioneer ablated animals, with schematic (below). L1 images were taken because there were no available promoters to image OLL in embryos. Spinning disk confocal maximum intensity projections shown (Ctrl n=8 animals; Ablation n=20 animals). **t-v,** As for (**q-s**) but for S3 neuron AIY (Ctrl n=10 animals; Ablation n=16 animals). **w-y,** As for (**q-s**) but for unassigned neuron AIB (Ctrl n=6 animals; Ablation n=9 animals). Note that the AIB outgrowth defect in embryogenesis (**h**) persists to L1 (**y**). **z,** Quantification of the percentage of AIB neurons with defective morphologies in L1 animals for control and pioneer ablated animals. ‘n’ = number of animals scored. ***p=0.0002 by two-sided Fisher’s exact test between Ctrl and Ablation. For cell specific labeling of neurons, see Methods and Supplementary Tables 2 and 3. Scale bar (10 μm) applies to panels (**b-c,g-h,k-l,r-s,u-v,x-y**), and timing for all panels is mpf. Neurons are colored according to which strata they belong (S1-Red, S2-Purple, S3-Blue, S4-Green, Unassigned-Yellow).

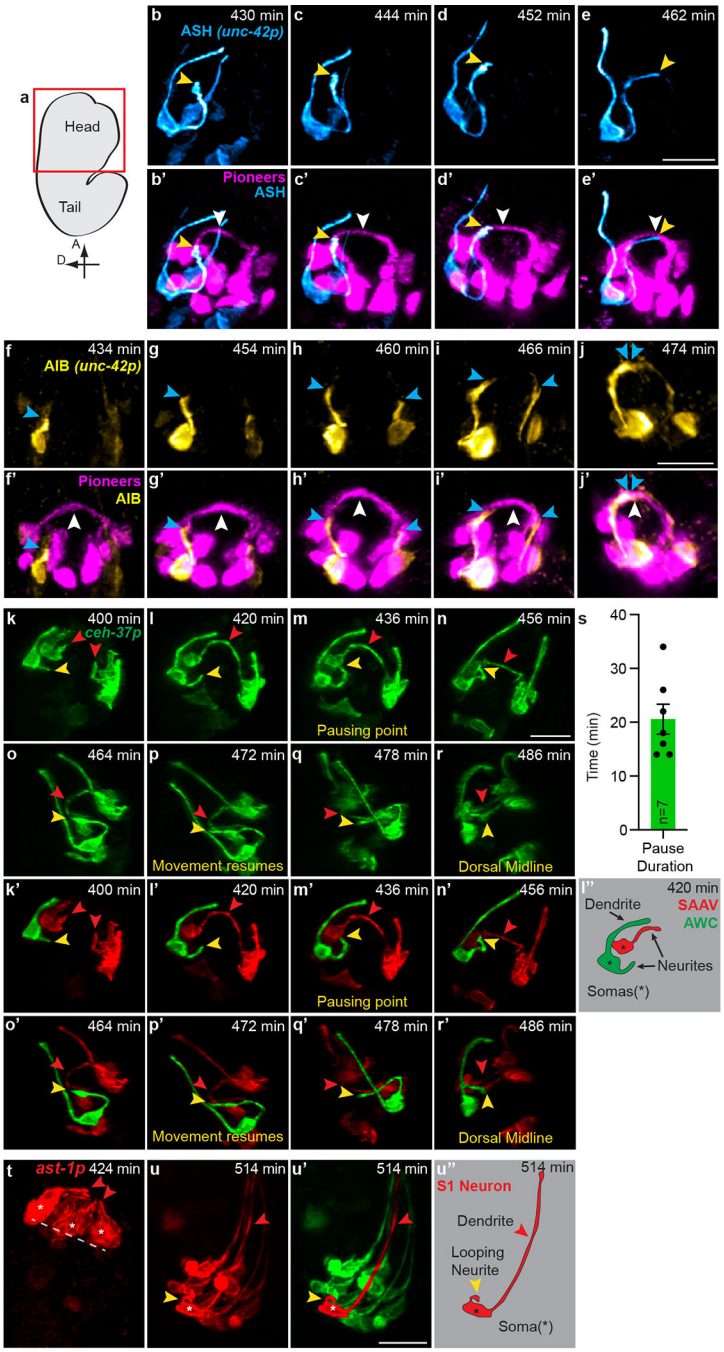

Extended Data Figure 10. A temporal progression of outgrowth, beginning with the S2 Pioneers, results in the inside-out development of the nerve ring.

a, Schematic of embryo, highlighting area in (**b-u**) as red rectangle. **b-e,** Time-lapse of the outgrowth dynamics of S3 neuron ASH in control animal. For ASH cell-specific labeling see Methods. **b'-e',** As (**b-e**) but includes S2 pioneer neurons (labeled with *lim-4p::mCherry*). Yellow arrowheads mark ASH axonal outgrowth in the context of the pioneers. White arrowheads mark dorsal midline. ASH outgrowth into the neuropil occurs after the pioneers have grown into the nerve ring. Deconvolved diSPIM maximum intensity projections shown

(n=4 embryos). **f-j,** Time-lapse of the outgrowth dynamics of unassigned neuron AIB in control animal. For AIB cell-specific labeling see Methods. **f'-j',** As (**f-j**) but includes S2 pioneer neurons (labeled with *lim-4p::mCherry*). Blue arrowheads mark AIB axonal outgrowth in the context of the pioneers. White arrowheads mark dorsal midline. Note that AIB enters the neuropil after the pioneers have reached the dorsal midline, and as ASH reaches the dorsal midline (compare **e'** to **h'**). Data collected in this way (**b-j**) were used for indicated neurons in Fig. 4j. Deconvolved diSPIM maximum intensity projections shown (n=6 embryos). **k-r,** Time-lapse of the outgrowth dynamics for S2 pioneer SAAV, and S4 neuron AWC. In (**k**) red arrowheads mark outgrowth of SAAV. In (**l-r**) red arrowheads mark dorsal midline and yellow arrowheads mark outgrowth of AWC. The S4 neuron AWC pauses for ~20 min near the SAAV soma before growing into the nerve ring. Deconvolved diSPIM maximum intensity projections shown. n=7 embryos. Note that *ceh-37p* promoter expresses strongly in SAAV and AWC, but weakly in ADF, AFD, AWB. **k'-r',** As (**k-r**) but one side of the bilateral AWC neurons have been pseudocolored green and the remaining image pseudocolored red to highlight the outgrowth of the S4 neurons (n=7 embryos; see Methods). **l",** Schematic of (**l'**) depicting the growing SAAV (red) and AWC (green) neuron. **s**, Quantification of AWC pausing duration. Each dot represents an embryo (n=7). AWC pauses at the SAAV cell body for ~20 min prior to entering the neuropil. Error bars are mean +/− SEM (see Materials and Methods for quantification). **t-u**, Time-lapse of the outgrowth dynamics for S1 sensory neurons. Red arrowheads mark sensory endings. Yellow arrowhead marks outgrowth of a looping neuron. Dashed line in (**t**) corresponds to the position of the pioneering neurons (seen in Fig 3i–j). Note how outgrowth of looping structures starts after 420 min, meaning, after the pioneer neurons have grown out (compare to Fig 3i–j). Image in **u** taken in a 3-fold embryo, which moved (therefore position of cell bodies different between **t** and **u**). Deconvolved diSPIM maximum intensity projections shown. (n=9 embryos; compare to Fig. 4j). **u',** As (**u**) but one S1 sensory neuron has been pseudocolored red and the remaining image pseudocolored green to highlight the looping outgrowth of the S1 neuron (see Methods). **u",** Schematic of (**u'**) depicting the growing loop of the S1 sensory neuron. Together, with the temporal dynamics of outgrowth, and the ablation studies, our findings support an inside-out model in which the strata are assembled through timed entry into the nerve ring. Starting with a core unit of the pioneering bundle, proceeding to central S2, then to the peripherally located neurons in S1 (anterior) and S4 (posterior), followed by outgrowth of neurons which link the strata, such as the S1 looping neurons or the neurons that cross strata (like AIB). Scale bar (10 μm) applies to panels (**b-e', f-j', k-r', t-u'**), and timing for all panels is mpf. Promoter used to drive expressing shown in italics in (**b, f, k, t**).

Supplementary Material

Refer to Web version on PubMed Central for supplementary material.

Acknowledgements

We thank Scott Emmons, Steve Cook, and Chris Brittin for sharing the segmented EM datasets and adjacency analysis code[18], and for helpful comments on this work. We thank Oliver Hobert for sharing the *ceh-48p* promoter and advice. We thank Zheng Zhou for sharing a 2xFYVE containing plasmid[54]. We thank David Hall for advice and help with electron microscopy images. We thank Ralf Sommer for use of an electron microscopy image.

We thank Henry 'Hank' Eden for comments on our manuscript. We thank members of the Colón-Ramos lab for insightful comments during manuscript preparation. We thank the Caenorhabditis Genetic Center (funded by NIH Office of Research Infrastructure Programs P40 OD010440) for *C. elegans* strains. We thank the Research Center for Minority Institutions program, the Marine Biological Laboratories (MBL), and the Instituto de Neurobiología de la Universidad de Puerto Rico for providing meeting and brainstorming platforms. H.S. and D.A.C-R. acknowledge the Whitman and Fellows program at MBL for providing funding and space for discussions valuable to this work. Research in the D.A.C-R., W.A.M., and Z. B. labs were supported by NIH grant No. R24-OD016474. M.W.M was supported by NIH by F32-NS098616. Research in H.S. lab was further supported by the intramural research program of the National Institute of Biomedical Imaging and Bioengineering (NIBIB), NIH. Research in Z.B. lab was further supported by an NIH center grant to MSKCC (P30CA008748). Research in the D.A.C.-R. lab was further supported by NIH R01NS076558, DP1NS111778 and by an HHMI Scholar Award.

Data Availability

The datasets generated during and/or analyzed during the study are available from the corresponding author upon request. To facilitate exploration of the placement of neurites in the C-PHATE diagrams we generated a 3D interactive version of the C-PHATE plots. Plots can be downloaded, and neurite condensation and position can be examined. These 3D interactive versions allow for identification of any neuron within the C-PHATE plot and provide iteration # and total neurons found within any cluster (See Supplementary Discussion 2 for instructions on how to access the data.)

References

1. Maynard DMOrganization of Neuropil. Am Zool2, 79–96 (1962).
2. Schurmann FWFine structure of synaptic sites and circuits in mushroom bodies of insect brains. Arthropod Struct Dev45, 399–421, doi:10.1016/j.asd.2016.08.005 (2016). [PubMed: 27555065]
3. White JG, Southgate E, Thomson JN & Brenner S The structure of the nervous system of the nematode Caenorhabditis elegans. Philos Trans R Soc Lond B Biol Sci 314, 1–340, doi:10.1098/rstb.1986.0056 (1986). [PubMed: 22462104]
4. Soiza-Reilly M & Commons KG Unraveling the architecture of the dorsal raphe synaptic neuropil using high-resolution neuroanatomy. Front Neural Circuits 8, 105, doi:10.3389/fncir.2014.00105 (2014). [PubMed: 25206323]
5. Zheng Zet al.A Complete Electron Microscopy Volume of the Brain of Adult Drosophila melanogaster. Cell174, 730–743 e722, doi:10.1016/j.cell.2018.06.019 (2018). [PubMed: 30033368]
6. Brugnone Net al. in 2019 IEEE International Conference on Big Data (Big Data). 2624–2633 (IEEE, 2019).
7. Kumar Aet al.Dual-view plane illumination microscopy for rapid and spatially isotropic imaging. Nat Protoc9, 2555–2573, doi:10.1038/nprot.2014.172 (2014). [PubMed: 25299154]
8. Wu Yet al.Spatially isotropic four-dimensional imaging with dual-view plane illumination microscopy. Nature biotechnology31, 1032–1038, doi:10.1038/nbt.2713 (2013).
9. Bao Zet al.Automated cell lineage tracing in Caenorhabditis elegans. Proceedings of the National Academy of Sciences of the United States of America103, 2707–2712, doi:10.1073/pnas.0511111103 (2006). [PubMed: 16477039]
10. Boyle TJ, Bao Z, Murray JI, Araya CL & Waterston RH AceTree: a tool for visual analysis of Caenorhabditis elegans embryogenesis. Bmc Bioinformatics 7, 275, doi:10.1186/1471-2105-7-275 (2006). [PubMed: 16740163]
11. Sulston JE, Schierenberg E, White JG & Thomson JN The Embryonic-Cell Lineage of the Nematode Caenorhabditis-Elegans. Developmental Biology 100, 64–119, doi:Doi 10.1016/0012-1606(83)90201-4 (1983). [PubMed: 6684600]
12. Azulay A, Itskovits E & Zaslaver A The C. elegans Connectome Consists of Homogenous Circuits with Defined Functional Roles. PLoS Comput Biol 12, e1005021, doi:10.1371/journal.pcbi.1005021 (2016). [PubMed: 27606684]

13. Chatterjee N & Sinha S Understanding the mind of a worm: hierarchical network structure underlying nervous system function in C. elegans. Prog Brain Res 168, 145–153, doi:10.1016/S0079-6123(07)68012-1 (2008). [PubMed: 18166392]
14. Cook SJet al.Whole-animal connectomes of both Caenorhabditis elegans sexes. Nature571, 63–71, doi:10.1038/s41586-019-1352-7 (2019). [PubMed: 31270481]
15. Towlson EK, Vertes PE, Ahnert SE, Schafer WR & Bullmore ET The rich club of the C. elegans neuronal connectome. J Neurosci 33, 6380–6387, doi:10.1523/JNEUROSCI.3784-12.2013 (2013). [PubMed: 23575836]
16. Varshney LR, Chen BL, Paniagua E, Hall DH & Chklovskii DB Structural properties of the Caenorhabditis elegans neuronal network. PLoS Comput Biol 7, e1001066, doi:10.1371/journal.pcbi.1001066 (2011). [PubMed: 21304930]
17. Yan Get al.Network control principles predict neuron function in the Caenorhabditis elegans connectome. Nature550, 519–523, doi:10.1038/nature24056 (2017). [PubMed: 29045391]
18. Brittin CA, Cook SJ, Hall DH, Emmons SW & Cohen N Volumetric reconstruction of main Caenorhabditis elegans neuropil at two different time points. bioRxiv, 485771, doi:10.1101/485771 (2018).
19. Brittin CA, Cook SJ, Hall DH, Emmons SW & Cohen N Beyond the connectome: A map of a brain architecture derived from whole-brain volumetric reconstructions. bioRxiv (2020).
20. Sabrin KM, Wei Y, van den Heuvel MP & Dovrolis C The hourglass organization of the Caenorhabditis elegans connectome. PLoS Comput Biol 16, e1007526, doi:10.1371/journal.pcbi.1007526 (2020). [PubMed: 32027645]
21. Kennerdell JR, Fetter RD & Bargmann CI Wnt-Ror signaling to SIA and SIB neurons directs anterior axon guidance and nerve ring placement in C. elegans. Development 136, 3801–3810, doi:10.1242/dev.038109 (2009). [PubMed: 19855022]
22. Rapti G, Li C, Shan A, Lu Y & Shaham S Glia initiate brain assembly through noncanonical Chimaerin-Furin axon guidance in C. elegans. Nat Neurosci 20, 1350–1360, doi:10.1038/nn.4630 (2017). [PubMed: 28846083]
23. Wadsworth WG, Bhatt H & Hedgecock EM Neuroglia and pioneer neurons express UNC-6 to provide global and local netrin cues for guiding migrations in C. elegans. Neuron 16, 35–46, doi:10.1016/s0896-6273(00)80021-5 (1996). [PubMed: 8562088]
24. Yoshimura S, Murray JI, Lu Y, Waterston RH & Shaham S mls-2 and vab-3 Control glia development, hlh-17/Olig expression and glia-dependent neurite extension in C. elegans. Development 135, 2263–2275, doi:10.1242/dev.019547 (2008). [PubMed: 18508862]
25. Blondel VD, Guillaume JL, Lambiotte R & Lefebvre E Fast unfolding of communities in large networks. J Stat Mech-Theory E, doi:Artn P10008 10.1088/1742-5468/2008/10/P10008 (2008).
26. Dasgupta A, Hopcroft J, Kannan R & Mitra P Spectral clustering by recursive partitioning. Lect Notes Comput Sc 4168, 256–267 (2006).
27. Kaufman L & Rousseeuw PJ Finding groups in data : an introduction to cluster analysis. (Wiley, 2005).
28. Moon KRet al.Visualizing structure and transitions in high-dimensional biological data. Nature biotechnology37, 1482–1492, doi:10.1038/s41587-019-0336-3 (2019).
29. Bargmann CIChemosensation in C. elegans. WormBook, 1–29, doi:10.1895/wormbook.1.123.1 (2006).
30. Goodman MBMechanosensation. WormBook, 1–14, doi:10.1895/wormbook.1.62.1 (2006).
31. Goodman MB & Sengupta P How Caenorhabditis elegans Senses Mechanical Stress, Temperature, and Other Physical Stimuli. Genetics 212, 25–51, doi:10.1534/genetics.118.300241 (2019). [PubMed: 31053616]
32. Newman MEModularity and community structure in networks. Proceedings of the National Academy of Sciences of the United States of America103, 8577–8582, doi:10.1073/pnas.0601602103 (2006). [PubMed: 16723398]
33. Millard SS & Pecot MY Strategies for assembling columns and layers in the Drosophila visual system. Neural Dev 13, doi:ARTN 11 10.1186/s13064-018-0106-9 (2018).
34. Sanes JR & Zipursky SL Design principles of insect and vertebrate visual systems. Neuron 66, 15–36, doi:10.1016/j.neuron.2010.01.018 (2010). [PubMed: 20399726]

35. Baier HSynaptic laminae in the visual system: molecular mechanisms forming layers of perception. Annu Rev Cell Dev Biol29, 385–416, doi:10.1146/annurev-cellbio-101011-155748 (2013). [PubMed: 24099086]
36. Ware RW, Clark D, Crossland K & Russell RL Nerve Ring of Nematode Caenorhabditis-Elegans - Sensory Input and Motor Output. J Comp Neurol 162, 71–110, doi:DOI 10.1002/cne.901620106 (1975).
37. Ward S, Thomson N, White JG & Brenner S Electron microscopical reconstruction of the anterior sensory anatomy of the nematode Caenorhabditis elegans.?2UU. J Comp Neurol 160, 313–337, doi:10.1002/cne.901600305 (1975). [PubMed: 1112927]
38. Riddle DLCelegans II (Cold Spring Harbor Laboratory Press, 1997).
39. White JClues to basis of exploratory behaviour of the C. elegans snout from head somatotropy. Philos Trans R Soc Lond B Biol Sci373, doi:10.1098/rstb.2017.0367 (2018).
40. Groh JMMaking space : how the brain knows where things are. (The Belknap Press of Harvard University Press, 2014).
41. Kaas JHTopographic maps are fundamental to sensory processing. Brain Res Bull44, 107–112, doi:10.1016/s0361-9230(97)00094-4 (1997). [PubMed: 9292198]
42. Sasakura H & Mori I Behavioral plasticity, learning, and memory in C. elegans. Curr Opin Neurobiol 23, 92–99, doi:10.1016/j.conb.2012.09.005 (2013). [PubMed: 23063296]
43. Chalfie Met al.The neural circuit for touch sensitivity in Caenorhabditis elegans. The Journal of neuroscience : the official journal of the Society for Neuroscience5, 956–964 (1985). [PubMed: 3981252]
44. Gray JM, Hill JJ & Bargmann CI A circuit for navigation in Caenorhabditis elegans. Proceedings of the National Academy of Sciences of the United States of America 102, 3184–3191, doi:10.1073/pnas.0409009101 (2005). [PubMed: 15689400]
45. Lockery SRNeuroscience: A social hub for worms. Nature458, 1124–1125, doi:10.1038/4581124a (2009). [PubMed: 19407792]
46. Macosko EZet al.A hub-and-spoke circuit drives pheromone attraction and social behaviour in C. elegans. Nature458, 1171–1175, doi:10.1038/nature07886 (2009). [PubMed: 19349961]
47. White JG, Southgate E, Thomson JN & Brenner S Factors That Determine Connectivity in the Nervous-System of Caenorhabditis-Elegans. Cold Spring Harb Sym 48, 633–640, doi:Doi 10.1101/Sqb.1983.048.01.067 (1983).
48. Wakabayashi T, Kitagawa I & Shingai R Neurons regulating the duration of forward locomotion in Caenorhabditis elegans. Neuroscience research 50, 103–111, doi:10.1016/j.neures.2004.06.005 (2004). [PubMed: 15288503]
49. Duncan LHet al.Isotropic Light-Sheet Microscopy and Automated Cell Lineage Analyses to Catalogue Caenorhabditis elegans Embryogenesis with Subcellular Resolution. J Vis Exp, doi:10.3791/59533 (2019).
50. Guo Met al.Rapid image deconvolution and multiview fusion for optical microscopy. Nature biotechnology, doi:10.1038/s41587-020-0560-x (2020).
51. Santella Aet al.WormGUIDES: an interactive single cell developmental atlas and tool for collaborative multidimensional data exploration. Bmc Bioinformatics16, doi:ARTN 189 10.1186/s12859-015-0627-8 (2015).
52. Ayala R, Shu T & Tsai LH Trekking across the brain: the journey of neuronal migration. Cell 128, 29–43, doi:10.1016/j.cell.2006.12.021 (2007). [PubMed: 17218253]
53. Chelur DS & Chalfie M Targeted cell killing by reconstituted caspases. Proceedings of the National Academy of Sciences of the United States of America 104, 2283–2288, doi:10.1073/pnas.0610877104 (2007). [PubMed: 17283333]

Online only references

54. Lu N, Yu XM, He XW & Zhou Z Detecting Apoptotic Cells and Monitoring Their Clearance in the Nematode Caenorhabditis elegans. Methods Mol Biol 559, 357–370, doi:10.1007/978-1-60327-017-5_25 (2009). [PubMed: 19609769]

55. Brandes Uet al.On Modularity Clustering. IEEE Transactions on Knowledge and Data Engineering20, 172–188, doi:10.1109/TKDE.2007.190689 (2008).
56. Wicks SR & Rankin CH Integration of mechanosensory stimuli in Caenorhabditis elegans. The Journal of neuroscience : the official journal of the Society for Neuroscience 15, 2434–2444 (1995). [PubMed: 7891178]
57. Walthall WW & Chalfie M Cell-cell interactions in the guidance of late-developing neurons in Caenorhabditis elegans. Science 239, 643–645, doi:10.1126/science.3340848 (1988). [PubMed: 3340848]
58. Kindt KSet al.Caenorhabditis elegans TRPA-1 functions in mechanosensation. Nat Neurosci10, 568–577, doi:10.1038/nn1886 (2007). [PubMed: 17450139]
59. Insley P & Shaham S Automated C. elegans embryo alignments reveal brain neuropil position invariance despite lax cell body placement. PloS one 13, e0194861, doi:10.1371/journal.pone.0194861 (2018). [PubMed: 29590193]
60. Shah PKet al.An In Toto Approach to Dissecting Cellular Interactions in Complex Tissues. Developmental cell43, 530–540 e534, doi:10.1016/j.devcel.2017.10.021 (2017). [PubMed: 29161596]
61. Coifman RR & Lafon S Diffusion maps. Applied and computational harmonic analysis 21, 5–30 %@ 1063–5203 (2006).
62. Hubert L & Arabie P Comparing Partitions. J Classif 2, 193–218, doi:Doi 10.1007/Bf01908075 (1985).
63. Gavish M, Nadler B & Coifman RR in ICML.
64. Le T, Yamada M, Fukumizu K & Cuturi M in Advances in neural information processing systems. 12304–12315.
65. Peyré G, Cuturi M & Solomon J in Proceedings of The 33rd International Conference on Machine Learning Vol. 48 (eds Florina Balcan Maria & Kilian Q. Weinberger) 2664–2672 (PMLR, Proceedings of Machine Learning Research, 2016).
66. Jaccard PTHE DISTRIBUTION OF THE FLORA IN THE ALPINE ZONE.1. New Phytologist11, 37–50, doi:10.1111/j.1469-8137.1912.tb05611.x (1912).
67. Gigante S, Charles AS, Krishnaswamy S & Mishne G in Advances in Neural Information Processing Systems. 1842–1853.
68. Schindelin Jet al.Fiji: an open-source platform for biological-image analysis. Nature methods9, 676–682, doi:10.1038/nmeth.2019 (2012). [PubMed: 22743772]
69. Belevich I, Joensuu M, Kumar D, Vihinen H & Jokitalo E Microscopy Image Browser: A Platform for Segmentation and Analysis of Multidimensional Datasets. PLoS biology 14, e1002340, doi:10.1371/journal.pbio.1002340 (2016). [PubMed: 26727152]
70. Kremer JR, Mastronarde DN & McIntosh JR Computer visualization of three-dimensional image data using IMOD. J Struct Biol 116, 71–76, doi:DOI 10.1006/jsbi.1996.0013 (1996). [PubMed: 8742726]
71. Moore JL, Du Z & Bao ZR Systematic quantification of developmental phenotypes at single-cell resolution during embryogenesis. Development 140, 3266–3274, doi:10.1242/dev.096040 (2013). [PubMed: 23861063]
72. Mello C & Fire A DNA transformation. Methods Cell Biol 48, 451–482 (1995). [PubMed: 8531738]
73. Murray JI, Bao Z, Boyle TJ & Waterston RH The lineaging of fluorescently-labeled Caenorhabditis elegans embryos with StarryNite and AceTree. Nat Protoc 1, 1468–1476, doi:10.1038/nprot.2006.222 (2006). [PubMed: 17406437]
74. Santella A, Du Z & Bao Z A semi-local neighborhood-based framework for probabilistic cell lineage tracing. Bmc Bioinformatics 15, 217, doi:10.1186/1471-2105-15-217 (2014). [PubMed: 24964866]
75. Armenti ST, Lohmer LL, Sherwood DR & Nance J Repurposing an endogenous degradation system for rapid and targeted depletion of C. elegans proteins. Development 141, 4640–4647, doi:10.1242/dev.115048 (2014). [PubMed: 25377555]

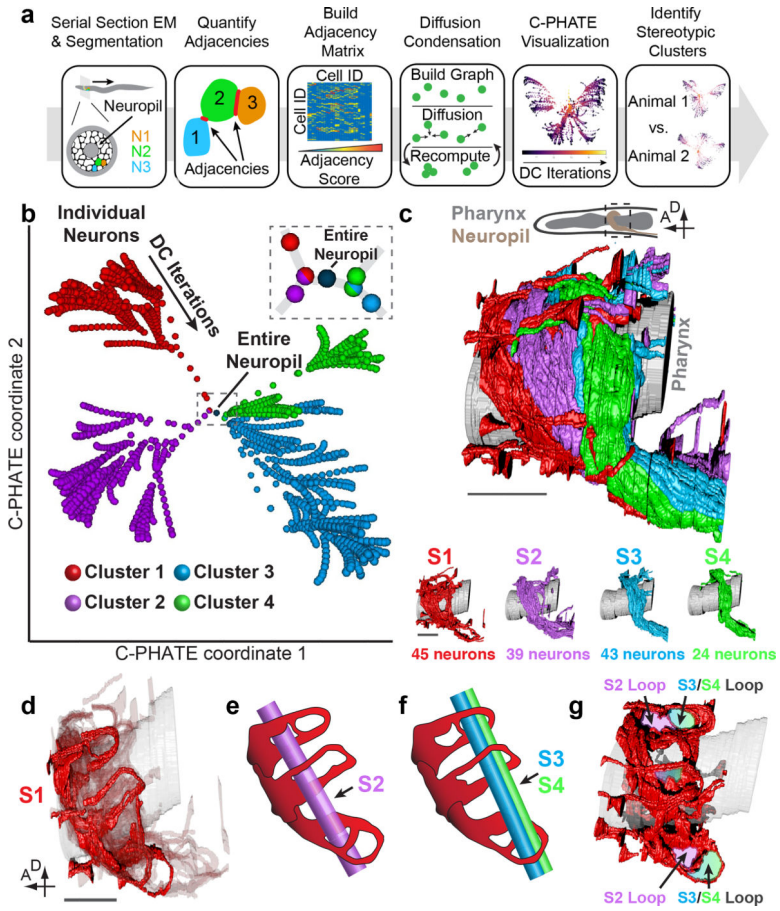

Figure 1: Computational detection of a hierarchical tree of neurite organization in the *C. elegans* neuropil.

a, Pipeline for analyses of the *C. elegans* neuropil. We used published serial section EM data[3] and previously quantified neuron-neuron contacts[18,19] to generate an adjacency matrix, which was analyzed via Diffusion Condensation (DC)[6] and visualized via C-PHATE[28]. L4 and adult animal outputs were quantitatively compared and stereotypic clusters and outliers identified. **b,** C-PHATE plot of DC analysis for L4 animal. Individual neurons are located at edges of the graph and condense as they move centrally. The four clusters identified are individually colored. Note that C3 and C4 are more closely related than C1 and C2 (Extended Data Fig. 2 a–d; Supplementary Videos 1–2) **c,** Volumetric reconstruction of the L4 *C. elegans* neuropil (from EM serial sections[3]) with the 4 strata individually colored. S1-S4 are stacked along the anterior-posterior axis, and S3 is basal to S4. Below are representations of individual strata (Extended Data Fig. 1c–h; Supplementary Video 3). **d,** Volumetric reconstruction of S1 perpendicular looping neurons (highlighted). **e,** Schematic representation of (**d**) with the trajectory of S2 (in **c**) through specific S1 loops. **f**, Like (**e**), but with Strata 3/4. **g,** The looping structure formed by 32 of the 45 S1 neurons, with loops colored according to encased strata (in **c**) (Extended Data Fig. 4 and Supplementary Videos 4–5). Scale bar is 5 μm in (**c**, **d**).

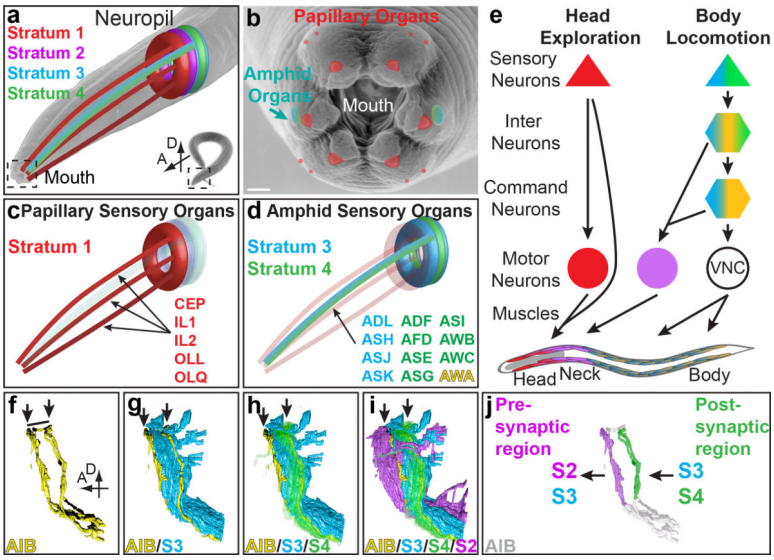

Figure 2: Neuropil architecture reflects functional segregation of sensory and motor outputs

a, Representation of head sensilla in the context of the four strata. Representation projected over a scanning EM of *C. elegans* (inset lower right), enlarged to show head sensilla and strata (Image from WormAtlas, produced by and used with permission of Ralf Sommer). **b,** Representation of head sensilla, projected over a scanning EM of the *C. elegans* mouth (corresponds to dashed box in lower-right of (**a**); image produced by and used with permission of David Hall). Scale bar is 1 μm**. c,** Schematic of papillary sensillum trajectories from mouth to neuropil. All papillary neurons cluster into S1. Individual neuron classes listed in lower-right. **d,** As (**c**), but with amphidial sensillum. BAG head sensory neurons excluded from analyses because they aren't in a sensillum[3]. **e,** Model of functional segregation of information streams within the neuropil. Papillary sensory information is processed in S1 and innervates head muscles to control head movement. Amphid sensory information is processed in S3/S4 and links to body muscles (via command interneurons in S3) and neck muscles (via motor neurons in S1/S2) to control body locomotion[29,38,42]. VNC is Ventral Nerve Cord. Interneurons cross strata to functionally link these modular circuits (Extended Data Fig. 5, and detailed version in Extended Data Fig. 3c). **f-i,** Volumetric reconstructions of the unassigned 'rich-club' AIB interneurons[15,20] in the context of nerve ring strata. Arrows indicate regions of AIB that border strata. AIB's proximal region borders S3/S4 (**g-h)**, and the distal region borders S2/S3 (**h-i**). Line in (**f**) indicates lateral region of AIB that shifts along the A-P axis to change strata. In (**h**) S4 is transparent to show AIB bordering S3/S4 (Supplementary Video 6). **j,** Volumetric rendering of the AIB pair. AIB is a unipolar neuron, with presynaptic specializations enriched in the distal region bordering S2/S3 and postsynaptic specializations enriched in the proximal region bordering S3/S4. Arrows indicate synaptic transmission flow (Extended Data Fig. 3g–k). Coloring of S1-Red, S2-Purple, S3-Blue, S4-Green, Unassigned-Yellow applied in (**a-j**).

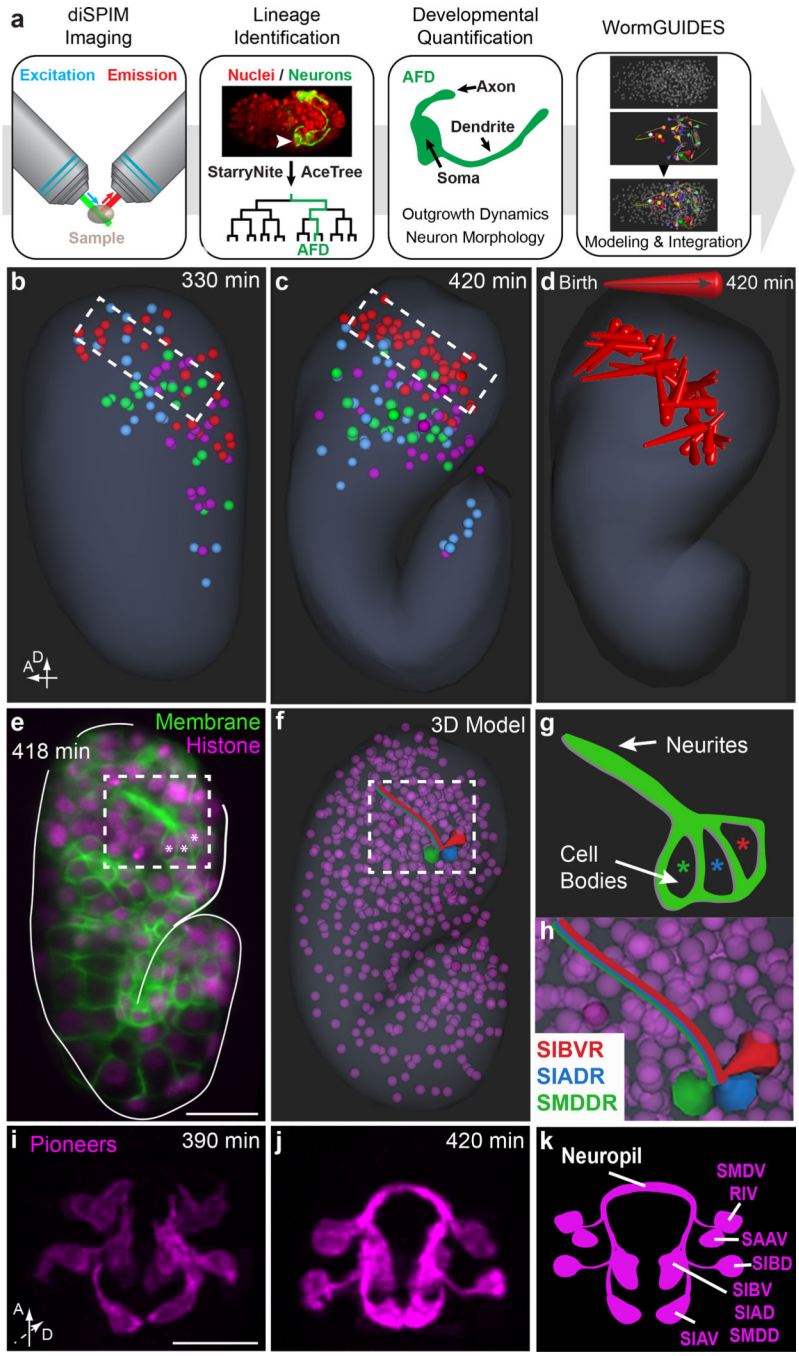

Figure 3. Developmental processes guide layered neuropil assembly

a, Analyses pipeline for *C. elegans* embryonic neurodevelopment. Embryonic neurodevelopment was imaged with the diSPIM[7,8,49,50], and cell lineages were determined via StarryNite[9] and AceTree[10]. Neuronal outgrowth and morphology were quantified, and information incorporated into the WormGUIDES atlas[51]. **b,** WormGUIDES atlas representation of all embryonic neuronal soma positions at 330 mpf. Somas are colored as in Fig. 1c to show their eventual neurite strata assignment. **c,** As, (**b**), but at 420 mpf. Dashed box in (**c**) as in (**b**), represents the final anterior position of the migrating S1 neurons

(Extended Data Fig. 7a–h; Supplementary Video 8). **d,** 3D depth trajectories of S1-cell movements between neuronal cell birth and 420 mpf. **e,** Comma stage embryo labeled with ubiquitous *nhr-2p::membrane::GFP* and *mCherry::Histone*. Asterisks denote the 3 lineaged cells. Image is single z-slice from a diSPIM arm (3 embryos were lineaged; Extended Data Fig. 8a–f; Supplementary Video 9). **f,** WormGUIDES atlas 3D model of the three cells observed in (**e**). **g,** Cartoon of the inset of the 3 cells observed in (**e**); asterisks denote somas of lineaged cells. **h,** Enlargement of inset (**f**), with early outgrowing cells identified via lineaging, listed and colored to highlight cellular locations. **i-k,** Time-lapse of the outgrowth dynamics of pioneer neurons and schematic (labeled with *lim-4p::membrane-tethered::GFP*; *lim-4p* embryonic expression was previously lineaged to the 8 neuron pairs listed in (**k**)[51]). Images are deconvolved diSPIM maximum intensity projections (n=16 embryos); Extended Data Fig. 8g–r; Supplementary Video 10. Scale bar (10 μm) applies to (**b-f, i-j**). Timing is mpf for all images.

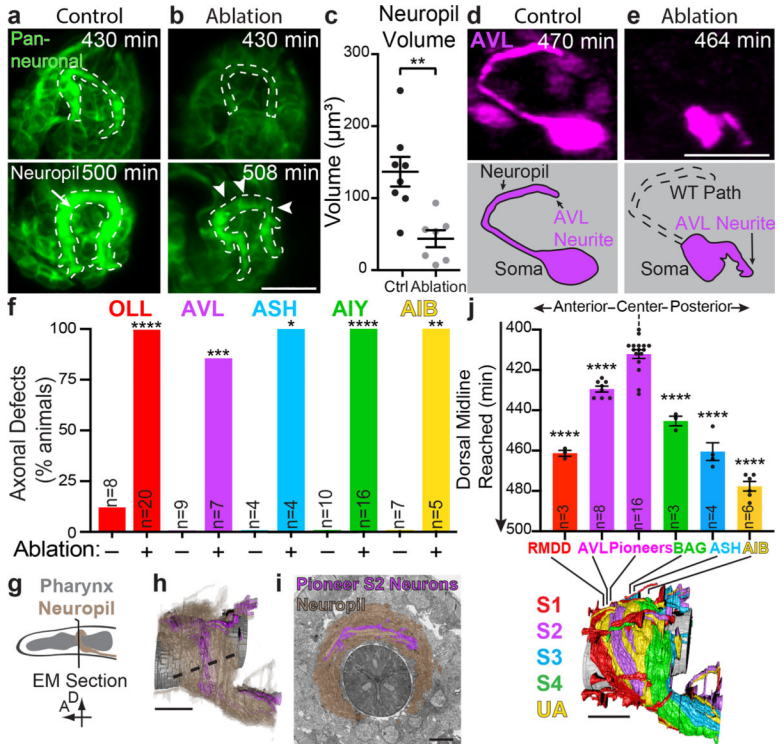

Figure 4. Temporal progression of outgrowth guided by pioneers results in inside-out neuropil development.

a-b, Neuropil development for control (**a**) or pioneer ablated (**b**) embryos monitored via pan-neuronal *ceh-48p::membrane-tethered::GFP*. Dashed lines represent the control neuropil (Ctrl n=8 embryos; Ablation n=7 embryos). Maximum intensity projections from one diSPIM arm (Supplementary Video 12). **c,** Quantification of neuropil volume for control or pioneer ablated animals. Dots in graph represent single embryos examined (Ctrl n=8; Ablation n=7). **p=0.0023 by unpaired two-tailed Student's t test between Ctrl and Ablation (Extended Data Fig. 8y–z). **d-e,** AVL development in control (**d**) or pioneer ablated (**e**) embryos monitored using an AVL-specific promoter (*lim-6p::GFP*). Dashed line depicts normal AVL outgrowth (Ctrl n=9 embryos; Ablation n=7 embryos). Deconvolved diSPIM maximum intensity projections shown (Supplementary Video 13). **f,** Quantification of neurite outgrowth for indicated neurons from each stratum in control and pioneer ablated animals. n= embryos (AVL, ASH, AIB) or L1 animals (OLL, AIY) scored. *p<0.05, **p<0.01, ***p<0.001, ****p<0.0001 by two-sided Fisher's exact test between Ctrl and Ablation for each neuron (see Methods for exact p-values; Extended Data Fig. 9). **g,** Schematic of worm head with position of EM cross-section (line) shown in (**h,i**). **h,** *C. elegans* L4 neuropil volumetric reconstruction. Centrally located S2 pioneers in purple, neuropil in brown, pharynx in grey. Dashed line indicates width of neuropil. **i,** Segmented serial section EM from[3] colored as in (**h**) (section corresponds to the L4 animal z-slice 54). Note that S2 pioneers are centrally located in the neuropil. Scale bar is 2.5 µm. **j,** Analysis of dorsal midline outgrowth for neurons from each stratum. Below is a volumetric neuropil reconstruction with the terminal location, along the dorsal midline, of the examined neurons. n= embryos scored. ****p<0.0001 by one-way ANOVA with Tukey's *post hoc* analysis between pioneers and each representative neuron. For statistical analysis of all pairwise

comparisons see Methods (Extended Data Fig. 10a–j). Timing for all panels is mpf, and error bars are mean +/− SEM. Color in (**d-f,j**) indicates the strata to which the neurons are assigned. Scale bar (10 μm) applies to (**a-b, d-e**); Scale bar (5 μm) applies to (**h,j**).